AD-A094 759 AIR FORCE INST OF TECH WRIGHT-PATTERSON AFB OH SCHOO--ETC F/G 20/13
A STUDY OF FREE CONVECTION IN AN INCLINED, RECTANGULAR CAVITY.(U)
DEC 80 M K KHAN
UNCLASSIFIED AFIT/GAE/AA/80D-13 NL

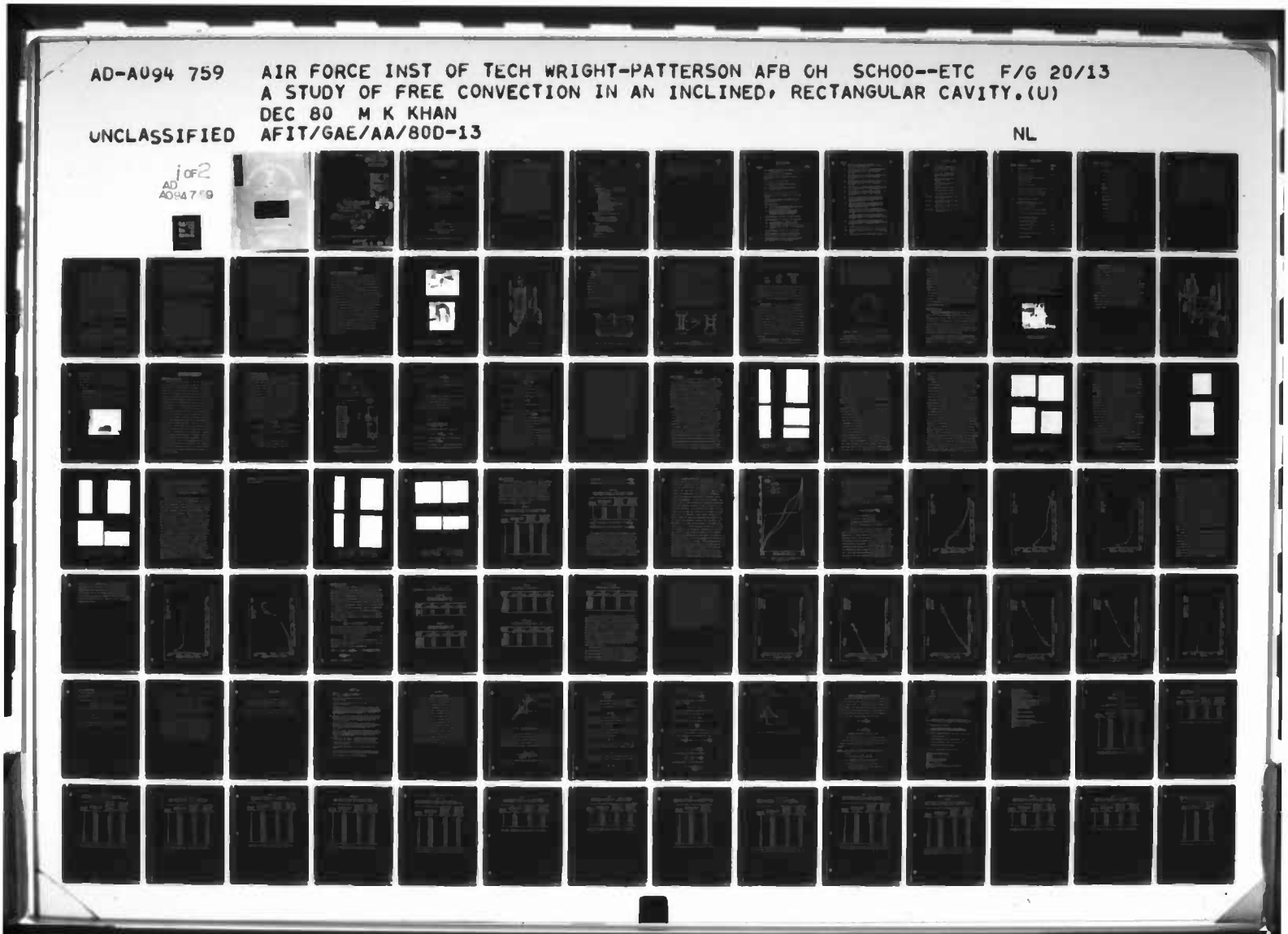

1 OF 2

AD A094759

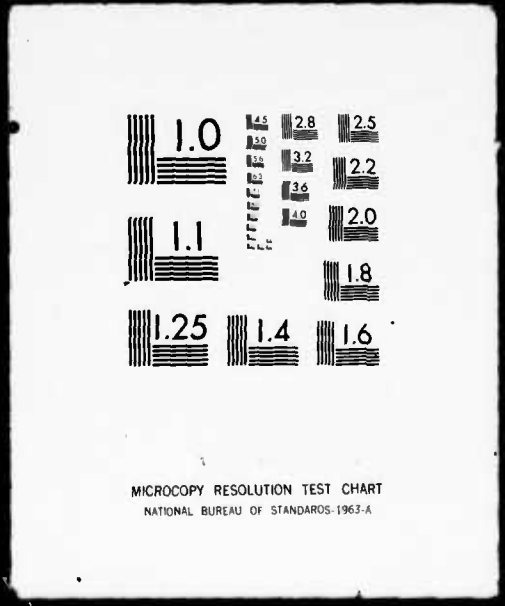

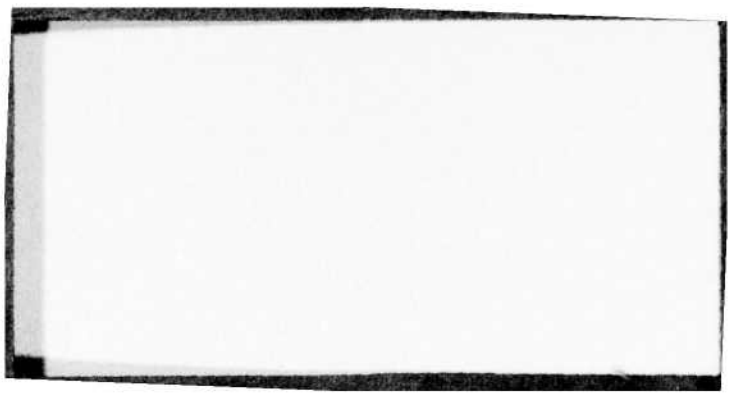

(14) AFIT/GAE/AA/80D-13

23 JAN 1981

APPROVED FOR PUBLIC RELEASE AFR 190-17.

Laurel A. Lampela

LAUREL A. LAMPELA, 2Lt, USAF
Deputy Director, Public Affairs

Air Force Institute of Technology (ATC)
Wright-Patterson AFB, OH 45433

Accession For	
NTIS GRA&I	☑
DTIC TAB	☐
Unannounced	☐
Justification	
By	
Distribution/	
Availability Codes	
Dist	Avail and/or Special
A	

(6) A STUDY OF FREE CONVECTION IN AN INCLINED, RECTANGULAR CAVITY.

(9) Master's THESIS,

AFIT/GAE/AA/80D-13

M. Khalid Khan
Flt. Lt. PAF

(10) Mohammad Khalid Khan

(11) Dec 80

(12) 108

DTIC ELECTE FEB 10 1981 S D F

Approved for public release; distribution unlimited.

012225

81 2 09 091

AFIT/GAE/AA/80D-13

A STUDY OF FREE CONVECTION IN AN INCLINED, RECTANGULAR CAVITY

THESIS

Presented to the Faculty of the School of Engineering
of the Air Force Institute of Technology
Air Training Command
in Partial Fulfillment of the
Requirements for the Degree of
Master of Science

by
Mohammad Khalid Khan
Flt. Lt. PAF
Graduate Aeronautical Engineering
December 1980

Preface

As part of this project, an apparatus was designed to study the free convection across an air layer, enclosed in a rectangular cavity, placed either in a vertical or an inclined position. Thanks is due to Mr. Carl Shortt and the school shop for the fabrication of the apparatus.

The temperature distributions in the air layer were measured optically with a Mach-Zehnder interferometer. I thank Mr. Bill Baker and Mr. Leroy Cannon for their assistance in conducting the experiment and Mr. Allen Hause of Aero-Propulsion Laboratory for his help in the use of a densitometer. I extend my thanks and deepest admiration to Dr. James E. Hitchcock of the Department of Aeronautics and Astronautics, Air Force Institute of Technology. His guidance and professionalism, both as a professor and an advisor, were greatly appreciated. Finally, I wish to acknowledge my gratefulness to my wife and son for their cheerful patience during this project.

Mohammad Khalid Khan

Contents

List of Figures

List of Tables

Nomenclature

Symbol	Definition	Units
A	Area of the Plate	ft^2
AR	Aspect Ratio, H/L	
c	Velocity of Light	ft/sec
d	Distance Between Two Fringes of Initial Pattern	ft
Gr	Grashof Number	
H	Height of Air Layer	ft
$\bar{h}$	Average Heat Transfer Coefficient .	$Btu/hr\text{-}ft^2\text{-}^oR$
k	Thermal Conductivity of Air at the Average Temperature $\frac{"T_H+T_c"}{2}$ . .	$Btu/hr\text{-}ft\text{-}^oR$
K_{DG}	Dale-Gladstone Constant	ft^3/lb_m
k_w	Thermal Conductivity of Air at the Wall Temperature	$Btu/hr\text{-}ft\text{-}^oR$
L	Width of Air Layer	ft
ℓ_1	Displacement of the First Fringe .	ft
ℓ_2	Displacement of the Second Fringe .	ft
$\overline{Nu}$	Average Nusselt Number	
P	Atmospheric Pressure	lb_f/ft^2
Q	Total Heat Transfer	Btu/hr
q_w	Local Heat Flux	$Btu/hr\text{-}ft^2$
R	Gas Constant of Air, 53.3	$ft\text{-}lb_f/lb_m\text{-}^oR$
Ra	Rayleigh Number	

Symbol	Definition	Units
T_1	Temperature at the Wall	^oR
T_2	Temperature at the First Fringe . .	^oR
T_3	Temperature at the Second Fringe .	^oR
T_c	Temperature at the Cold Wall . . .	^oR
T_H	Temperature at the Hot Wall	^oR
ΔT	Temperature Difference Between the Plates	^oR
$\frac{\partial T}{\partial Y}$	Temperature Gradient	^oR/ft
x	Distance Measured Along the Plate .	ft
y	Distance Measured Perpendicular to the Plate	ft
y_1	Distance of the First Fringe From the Wall	ft
y_2	Distance of the Second Fringe From the Wall	ft
λ_o	Wavelength of Undisturbed Light . .	μ m
λ_{vac}	Wavelength of Light in Vacuum . . .	μ m
ϕ	Angle of Inclination	degrees
τ	Period of Light Beam	μ sec

Abstract

A small experimental apparatus was designed for the measurement of heat flux across an enclosed, rectangular air cavity, which could be placed at any angle of inclination. The heat flux evaluation was done with the help of an interferometer. Heat flux was determined for five aspect ratios, each placed at four different angles and two different temperature differences for each setting. The average Nusselt number was found to be primarily a function of Grashof number or Rayleigh number. Three correlation equations developed by earlier studies are fitted to the data. The correlation equations are found to approximate the heat flux within ± 11%, up to a Grashof number of 1.2 million.

I. INTRODUCTION

Free convection between two vertical or inclined plates has recently become very important to the designers of solar collectors. Smaller collector areas can be used if heat loss can be reduced from the absorber plate through the cover plates. In other applications, the convection arising in such layers is utilized to transport heat. The problem of predicting the amount of heat transported through a vertical air layer has found considerable attention in the past. One of the first publications on the subject was written by W. Nusselt in 1909 (Reference 1). It was followed by a series of other papers, the most extensive ones by Mull and Reiher (Reference 2) and by DeGraaf and Van der Held (Reference 3). The primary aim of these papers was to measure the total amount of heat which is transported from the hot plate to the cold plate in a vertical geometry. The results were presented in the dimensionless form:

$$\overline{Nu} = C(Gr)^m \left(\frac{H}{L}\right)^n$$

where the mean Nusselt number $\overline{Nu}$, and the Grashof number Gr, are based on the width of the air layer L, and H is the height of the air layer. The exponents m and n acquire different values for laminar and turbulent flow.

The problem of predicting the amount of heat transfer between the hot and the cold plate of a horizontal,

rectangular geometry has also been studied to some extent (Reference 4). Important investigations of free convection across inclined air layers, with various angles of inclination, were carried out by DeGraaf and Van der Held (Reference 5) and by K. G. T. Hollands, T. E. Unny, G. D. Raithby and L. Konicek (References 6 and 7). However the authors have limited their studies to Rayleigh numbers ranging from 1000 to 100,000. The more recent work by K. G. T. Hollands and others (Reference 6) has provided a correlation of the form

$$\overline{Nu} = Nu(Ra \cos \phi)$$

where $\overline{Nu}$ is given as a function of Rayleigh number, $Ra = Gr \cdot Pr$, and the angle of inclination, ϕ.

The present study has been carried out with the objective of confirming the accuracy of the correlation equations developed for the average Nusselt number. In particular, it was desired to check their applicability for Grashof numbers greater than 100,000. For free convective heat transfer across inclined air layers, the correlation equation developed by K. G. T. Hollands and others (Reference 6) has been used. For heat transfer across vertical air layers, the correlation equations developed by E. R. G. Eckert and Walter O. Carlson (Reference 8) have been used.

In this research free convection has been studied for five different aspect ratios, H/L = 11.295, 7.867,

3.933, 1.967, 0.929, and at four different angles, ϕ = 0, 30, 60, and 90 degrees. In any of the inclined positions, the hot surface remained below. The study has been carried out for two different temperature differences for each geometry and angle. Gas temperature measurements were made optically with the help of a Mach-Zehnder Interferometer. An apparatus was designed for the purpose of this experiment which consists of two copper plates, each one foot long, six inches wide, and a quarter inch thick. The hollow plates were kept at a constant temperature with the help of running cold or hot water through the respective plates. Wood blocks separate the copper plates, and optical glass plates seal the ends of the rectangular enclosure. A detailed description of the apparatus is given in Section II. The experimental procedures and the data reduction techniques are included in Section III.

It was proved that Eckert's correlation for free convective heat transfer between two vertical plates and Hollands' correlation for free convection between two inclined or horizontal plates hold good at Rayleigh numbers as high as one million. A general pattern for the distribution of the local Nusselt numbers was observed; but since there was a lot of scatter in the data, these results are not as dependable as the mean Nusselt number data. A detailed discussion about the results is included in Section IV.

II. APPARATUS

Design Concept and Constraints

The apparatus was designed to be compatible with the 23 inches wide test section of a Mach-Zehnder interferometer. Also, because the interferometer has 7-inch diameter mirrors, the maximum length of the rectangular cavity was constrained to 6 inches. The layout of the apparatus is given in Figure 1(a). The apparatus can be seen in detail in Figure 1(b) and Figure 2. The apparatus was designed so that the cavity could be rotated to any desired angle from the horizontal. Both ends of the cavity have been manufactured from hard wood, so that adiabatic end-boundary conditions could be approached. Interchangeable blocks of various size determine the aspect ratio of the cavity. The optical path length, 12 inches, was chosen to produce reasonable interference fringe deflections for temperature differences up to 35°F between the isothermal plates. Optical glass plates at each end complete the enclosure. The temperatures of the hot and the cold copper plates are maintained constant with the help of running constant temperature hot or cold water through them, respectively.

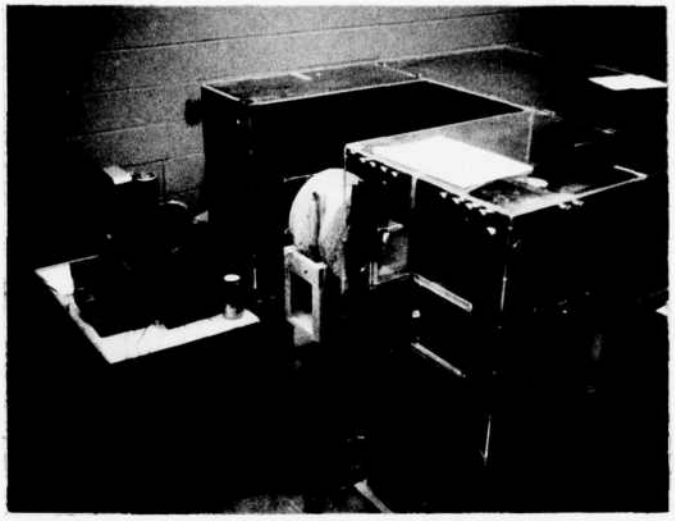

(a)

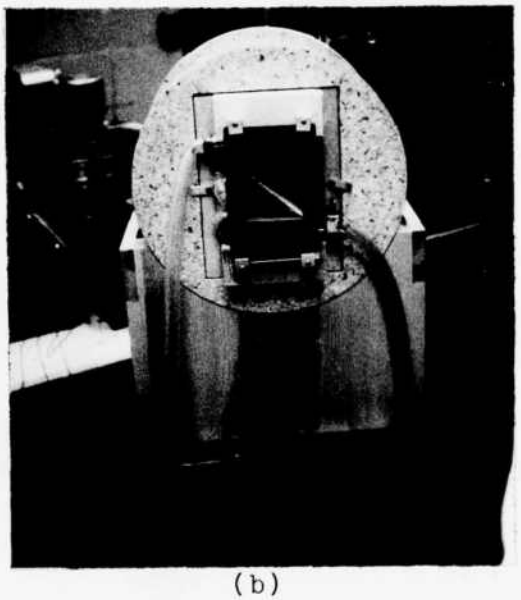

(b)

Figure 1

a) A general view of the apparatus and the interferometer.
b) Front view of the apparatus.

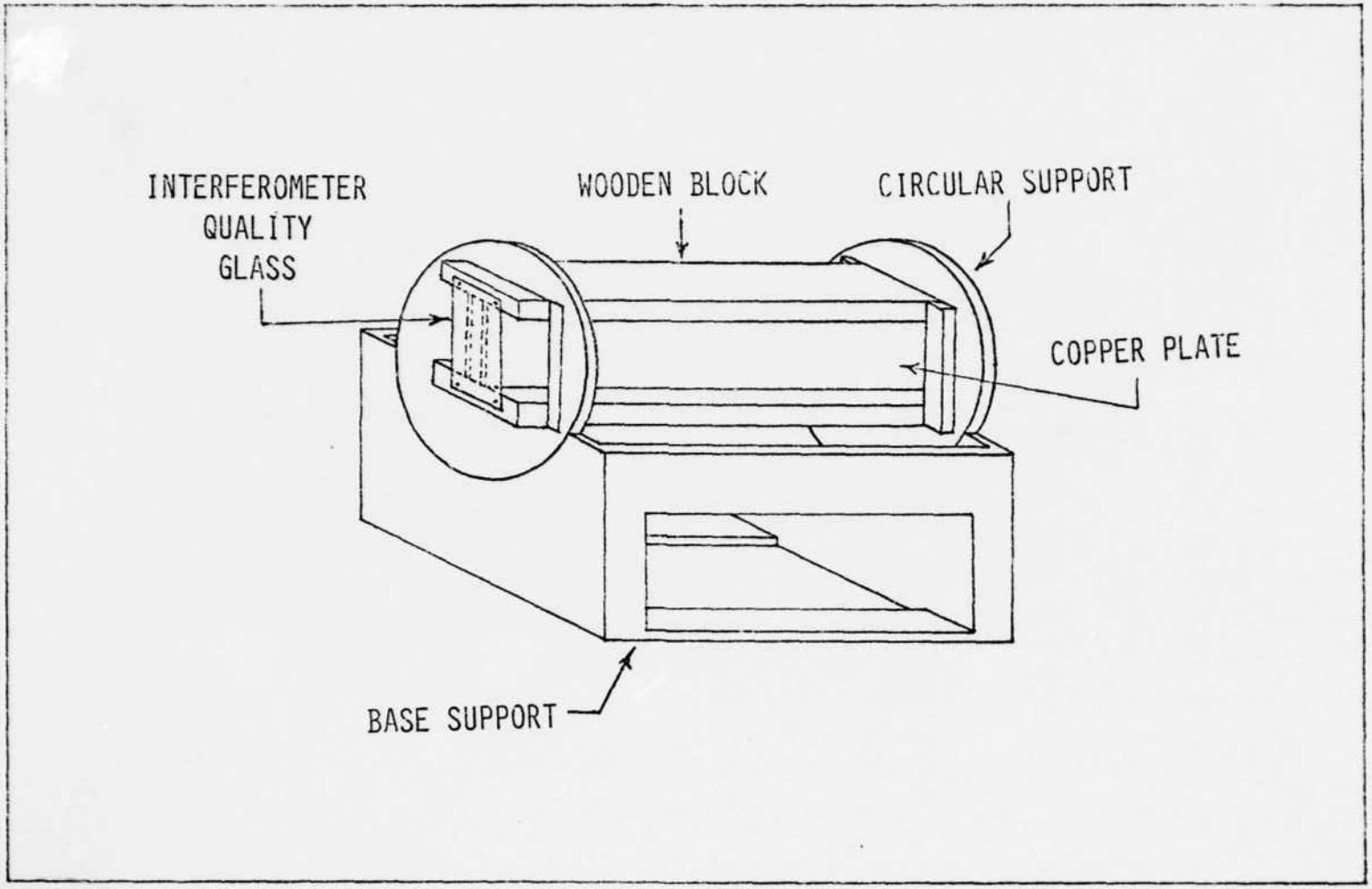

Figure 2 . An unscaled 3-dimensional drawing of the apparatus.

Design Details and Description of the Apparatus

An unscaled three-dimensional drawing of the apparatus is shown in Figure 2.

Copper plates. Two copper plates, each one foot long, six inches wide and one-quarter inch thick, have been used for the hot and the cold surfaces of the rectangular cavity to be studied. The copper plates have channels built into each plate to form a hollow body. Each plate has a flow channel entrance and exit at diagonally opposite corners. These have been formed by drilling holes through the outer skin of the plates and then welding a 5/8" external diameter, 1/2" long copper pipe to the plates over the holes. A sketch of the plate is presented in Figure 3. To minimize external heat loss, the hot plate has been covered externally with loose glass-wool.

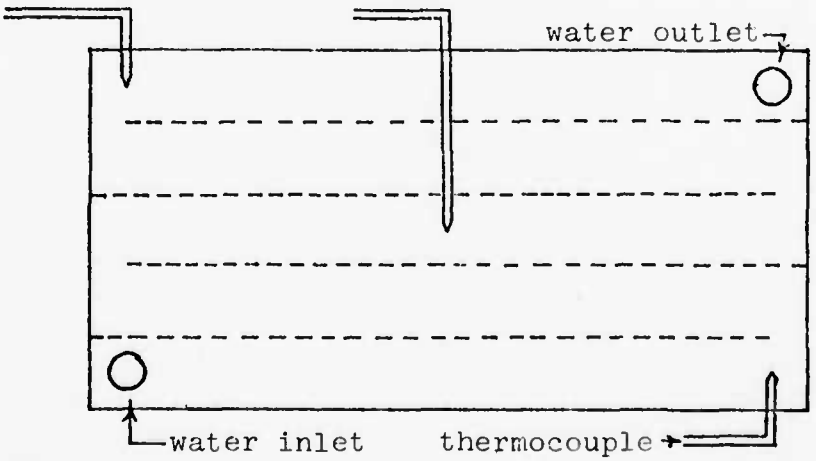

Figure 3. Top View of the Copper Plate.

Thermocouples. Copper-constantan thermocouples were soldered at three points into drilled cavities on the external surface of each plate, as shown in Figure 3. A negligible temperature difference between the inner and outer surfaces of the plates can be assumed because of the high thermal conductivity of copper.

Wooden blocks. The one-foot long sides of the copper plates were inserted into two grooved wooden blocks at both the sides, thus forming a rectangular cavity with copper plates on two sides and wooden blocks on the other two sides. Figure 4(a) shows an assembled cross-sectional view of the 5.9" x 1.5" geometry. The other three geometries having a 5.9" height look similar. Figure 4(b) shows the cross-sectional view of the 2.786" x 3.00" geometry.

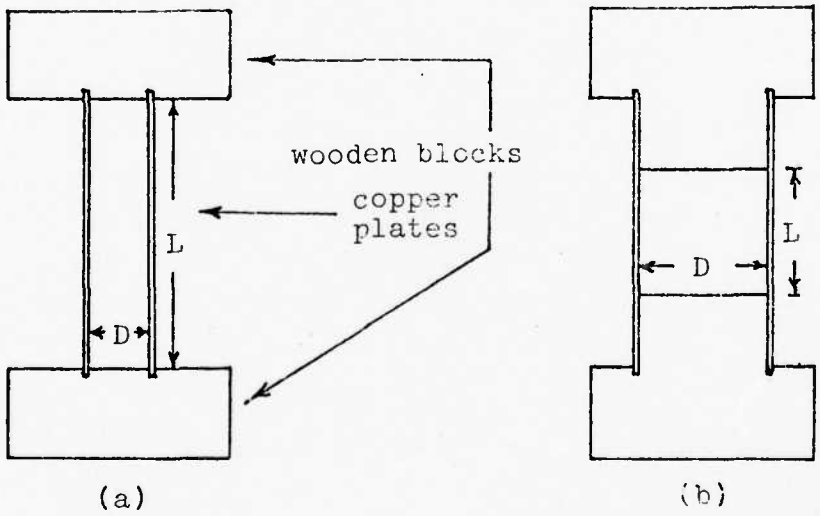

Figure 4
a) End View of Rectangular Cavity, 5.9" x 1.5".
b) End View of Rectangular Cavity, 2.786" x 3.00".

The five different cross-sections thus formed are listed below.

H	L	Aspect Ratio
5.93"	0.525"	11.295
5.9"	0.75"	7.867
5.9"	1.5"	3.933
5.9"	3.00"	1.967
2.786"	3.00"	0.929

The grooves where the copper plates fit into the wooden blocks have a lining of soft, spongy material so that air leaks from the rectangular cavity are minimal. The two wooden blocks are held together by four wooden strips on the outer side of the copper plates so that the system is rigid.

Glass plates. Both open ends of the rectangular cavity formed by the copper plates and the wooden blocks are closed with the help of 1/4" thick, interferometer quality glass plates. These glass plates are of high quality, no air bubbles or other constructional deformations, and have uniform thickness. The glass plates are held in place by four metallic clamps which are screwed into the wooden blocks. See Figure 1(b). Soft material lining is placed between the glass plates and the wooden blocks to minimize air leaks. Care was taken while placing the lining so that the view of the cavity was not obstructed.

Circular end supports. The assembly of copper plates, wooden blocks, and glass plates was supported at both the

front and the rear ends by two circular supports, 1.5" thick. As shown in Figure 5, these are 14.5" diameter with a 7.5" x 10" rectangle cut out from their centers. One of the circular supports is graduated into 360° and marked at 15° increments. The 0° and 180° graduations are exactly perpendicular to the copper plates, and the 90° and 270° graduations are exactly parallel to the copper plates.

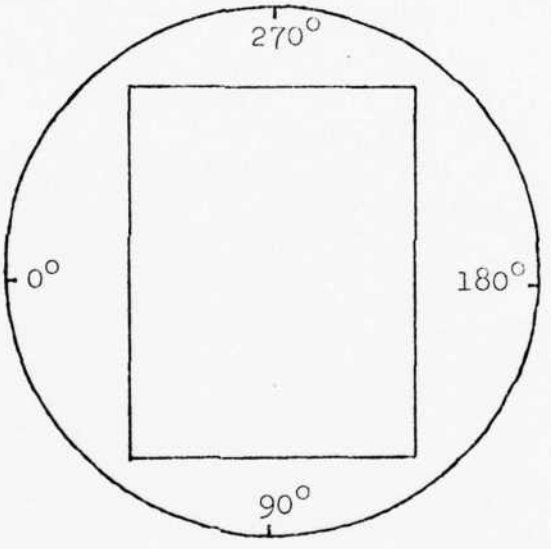

Figure 5. Front View of the Circular End-Support.

Base support. The base-support, as shown in Figure 1, has two semi-circular mounts. The circular end-supports rest on top of these semi-circular mounts. Thus by

rotating the circular end-supports in the semi-circular base support, the copper plates can be placed at any desired angle. An arrow mark has been drawn on the semi-circular base-support in such a way that when 0^{o} graduation of the circular end-support is in line with this mark, the copper plates are exactly horizontal. The circular end-supports can be rotated to any other angle by simply aligning that particular angle on the circular end-support with the mark on the base-support. The whole apparatus once assembled was placed on top of an adjustable tripod, as shown in Figure 1(a), and can be rotated and moved up and down. These adjustments were made to align the axis of the rectangular cavity parallel to and centered in the interferometer light beam.

Other Accessories

Temperature measurement apparatus. The thermocouples were connected to a Rubicon Potentiometer, through a multi-terminal junction box. The operation of the potentiometer is explained in Reference 12. The cold junction of the thermocouples was kept at $32^{o}F$ with the help of an ice-bath. The millivolts reading of the potentiometer can be converted to temperature reading through standard copper-constantan thermocouple conversion table.

Precision constant temperature circulating system. Constant temperature hot water was provided by a constant temperature circulating system. The system consists of a

2 1/2 gallon tank, electric heating coils, a stirrer and an electric pump. The device also has an "Adjustable Micro-Set Thermoregulator", which can keep the temperature of the circulating hot water constant within $\pm$ 0.02°F. The maximum rated temperature is 210°F. The temperature of the water in the bath can be noted by inserting a thermometer into the bath through a hole meant for that purpose. Complete operating instructions are available in Reference 9. A picture of the system is provided, Figure 6.

Cold tap-water was circulated through the cold plate.

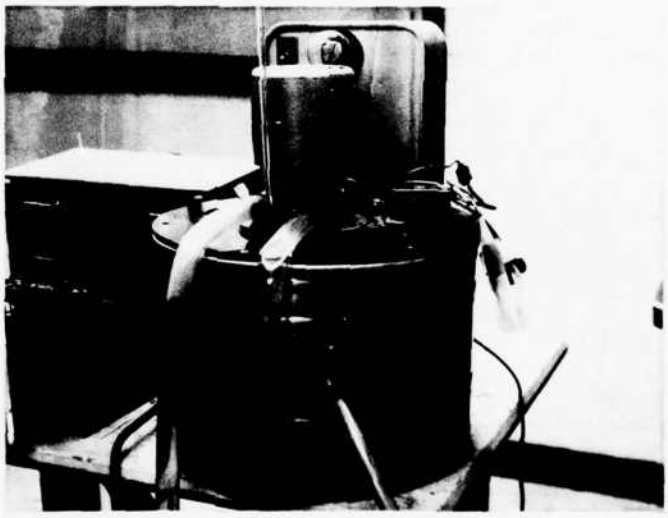

Figure 6. Precision Constant Temperature Circulating System.

Interferometer. A Mach-Zehnder interferometer was used to measure the gas temperatures in the rectangular cavity. A schematic diagram of this instrument is given in Figure 7. Monochromatic light from source S is made parallel by a parabolic mirror M and is divided by a beam splitter S_1, which is a semi-transparent mirror. The reflected beam proceeds to plane mirror M_2. The two beams are combined by splitter plate S_2, which is identical with S_1. The test section is between M_2 and S_2. When the instrument is properly adjusted, these beams produce interference fringes which are then focused on the screen or camera I by parabolic mirror M_3. A detailed discussion about this instrument is available in References 10 and 11. A polaroid land camera was used to photograph the interference fringes.

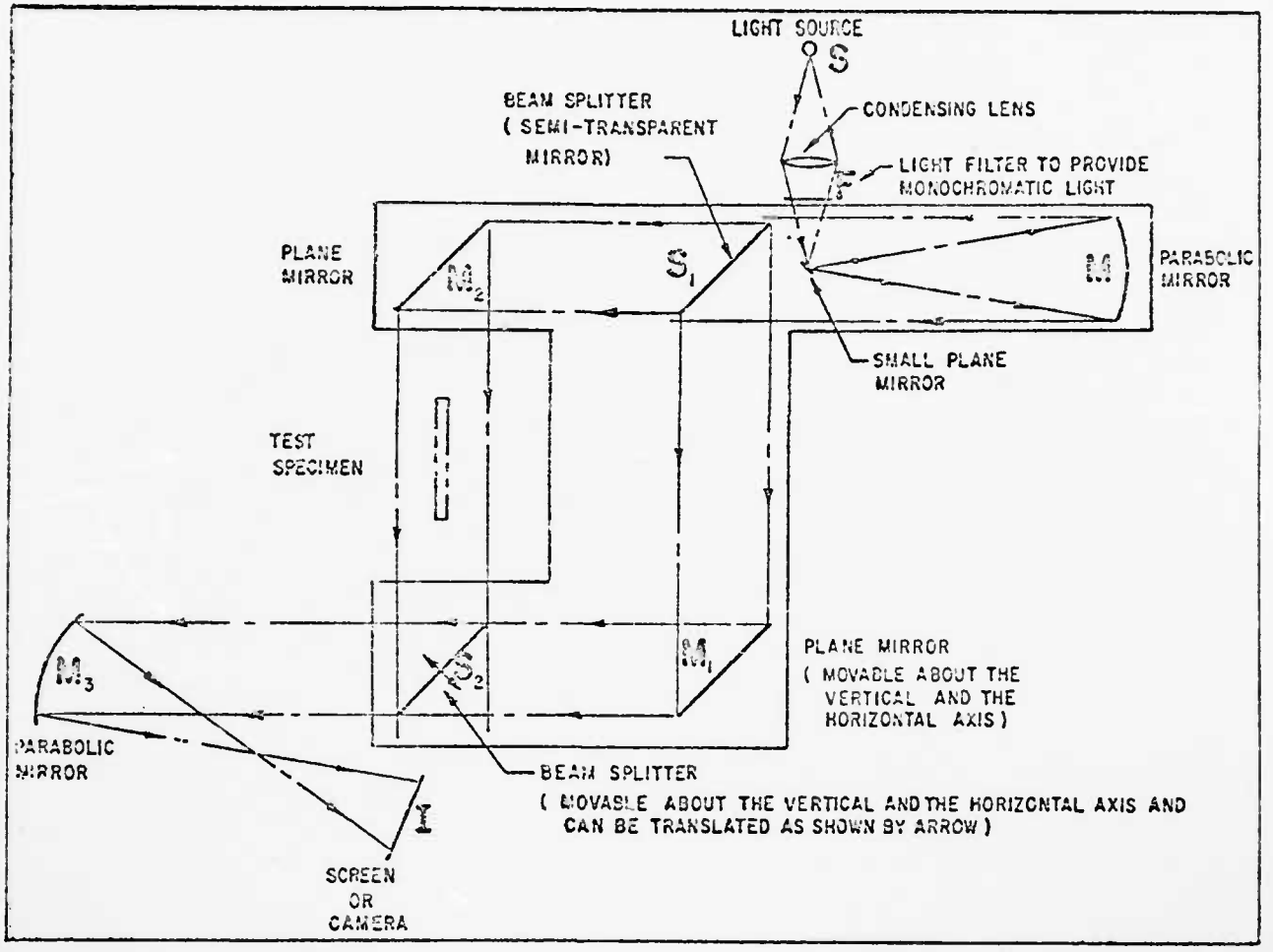

Figure 7. A schematic diagram of the Mach Zehnder interferometer.

Compensating glass. Since the light beam between M_2 and S_2 has to pass through two 1/4" thick glass plates of the test apparatus, it is therefore compensated by placing a 1/2" thick glass plate in the reference beam between M_1 and S_1. This is also a high quality glass plate with no air bubbles.

Microcomparator. This device was used to measure the distances on an interferogram (picture of the fringes from an interferometer). As shown in Figure 8, it is a microscope mounted on a traversing mechanism. A distance on an interferogram can be measured to ten thousandths of an inch with this device.

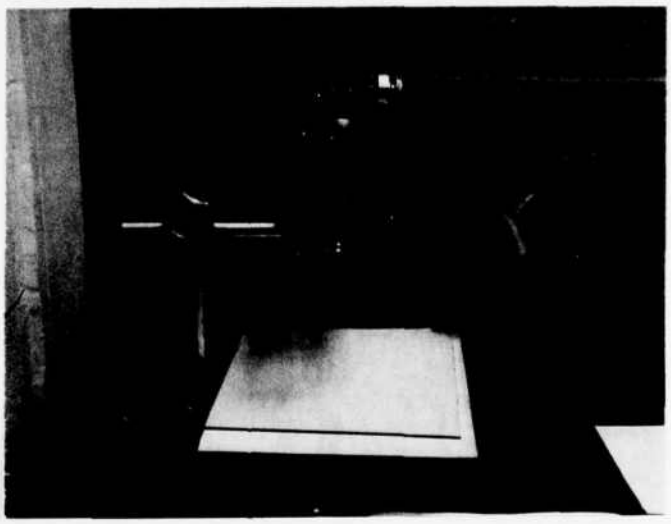

Figure 8. Microcomparator.

III. EXPERIMENTAL PROCEDURE AND DATA REDUCTION TECHNIQUE

Experimental Procedure

The apparatus, once placed in the test section, was adjusted on the tripod to align the axis of the rectangular cavity with the interferometer light beam. The copper plates were placed vertically for the first test at each aspect ratio, because that was the only position when the complete cross-section could be seen on the screen. The interferometer was adjusted to give a set of finite fringes, perpendicular to the copper plates, and a picture of fringes was taken in this position with a polaroid camera. Cold tap water was then circulated through the cold plate. The electrical resistance heaters in the constant temperature bath were turned on, and heated water was circulated through the hot plate. The desired steady-state thermal condition was obtained by adjusting the thermoregulator on the constant temperature bath. A picture of the resulting deflected finite fringe pattern was then taken. Output of the six copper-constantan thermocouples was recorded for the accurate determination of the copper plate temperatures. The thermoregulator was next set to a higher temperature, and the forementioned procedure was repeated. The apparatus was allowed to cool to room temperature before it was rotated to another angle of inclination. The interferometer was again adjusted to give a set of finite fringes perpendicular to the copper plates and the forementioned procedure was repeated.

Data Reduction Technique

Finite Fringe Method. The interferometer was adjusted so that alternate dark and light fringes were obtained as shown in Figure 9(a). This was done by rotating the splitter lens so that the two coherent wave fronts were combined at a small angle. The light was then in phase at the line of intersection and increasingly out of phase away from the line of intersection. Bright fringes occurred where the light was out of phase by 0, 1, 2, 3, ... , wavelengths, and dark fringes occurred at the points where the light was out of phase by 1/2, 1 1/2, 2 1/2, ... , wavelengths. Once the temperatures of the copper plates were varied, density variations occurred in the air layer enclosed between the plates, and the fringes in the test section were displaced as shown in Figure 9(b). It will be proved in Appendix A that if T_1 ($^{\circ}R$) is the temperature of the hot plate then

$$T_2 = \frac{T_1}{1 + \epsilon_1 C_1 T_1}$$

where T_2 = temperature at a distance y_1 from the plate ($^{\circ}R$)

y_1 = distance of the first fringe from the wall (ft)

$\epsilon_1 = \frac{\ell_1}{d}$

ℓ_1 = displacement of the first fringe from its initial position (inches)

d = distance between fringes (inches)

$$C_1 = \frac{(\lambda_o)(R)}{(L)(K_{DG})(P)}$$

λ_o = wavelength of light

K_{DG} = Dale-Gladstone constant

$$\frac{\lambda_o}{K_{DG}} = 4.91 \times 10^{-4} \frac{lb_m}{ft^2}$$

L = length of test section (one foot)

P = atmospheric pressure (lb_f/ft^2)

$$R = \text{gas constant for air} = 53.35 \frac{ft\text{-}lb_f}{lb_m\ ^oR}$$

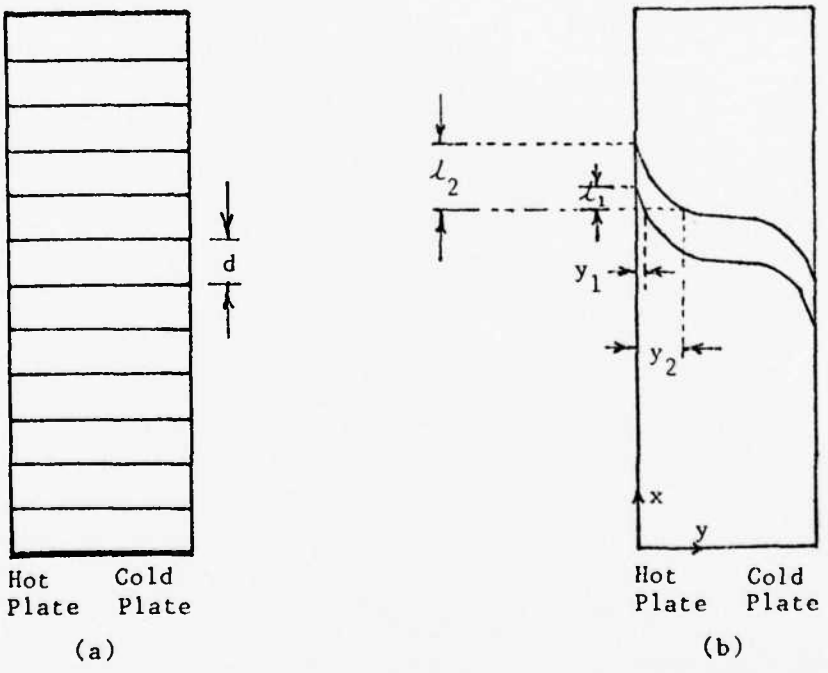

Figure 9

a) Initial fringe pattern when both plates are at equal temperature.

b) Fringe pattern when fringes are displaced because of temperature difference between the plates.

In a similar way

$$T_3 = \frac{T_1}{1 + \epsilon_2 C_1 T_1}$$

where T_3 = temperature at a distance y_2 from the plate ($^{\circ}R$)

y_2 = distance of the second fringe from the plate (ft)

$$\epsilon_2 = \frac{\ell_2}{d}$$

ℓ_2 = displacement of the second fringe from its initial position (inches)

Once the temperatures T_1 and T_2, at distances y_1 and y_2 from the plate, are known, then a second-order curve can be passed through these two points:

$$T = a + by + cy^2$$

where $a = T_1$

$$b = \frac{T_2 - T_1}{y_1} - cy_1$$

and $$c = \frac{y_2(T_2 - T_1) - y_1(T_3 - T_1)}{y_1 y_2 (y_1 - y_2)}$$

The local heat transfer at the wall, q_w, is then

$$q_w = - k_w \left.\frac{\partial T}{\partial y}\right|_{y=0} = - k_w b$$

where k_w = thermal conductivity of air at the wall temperature ($\frac{Btu}{hr\ ft\ ^{\circ}F}$)

The total heat transfer, Q, is determined by dividing the plate into small sections, determining the local heat

transfer for each section and numerically integrating the local heat transfers over the plate.

The average heat transfer is determined by

$$\bar{h} = \frac{Q}{A(T_H - T_C)}$$

where A = area of the plate (ft^2)

T_H = temperature of the hot plate (^oF)

T_C = temperature of the cold plate (^oF)

The average Nusselt number, $\overline{Nu}$, for the plate is then

$$\overline{Nu} = \frac{\bar{h}L}{k}$$

where L = width of the air layer between the two plates (ft)

k = thermal conductivity of air at the average temperature $\frac{"T_H + T_C"}{2}$ $(\frac{Btu}{hr\ ft\ ^oF})$

The above-mentioned technique for determining the average Nusselt number has been programmed for data processing, see Appendix B. The procedure for determining local heat transfer at the cold plate is similar.

A more accurate value of the average Nusselt number can be determined if the plate is subdivided into a large number of sections and the local heat transfer determined for each of those sections. For the four geometries having a height of 5.9" or more, the plate was divided into 20 sections, and for the geometry having a 2.786" height, the plate was divided into 8 sections.

The most difficult task in the whole project was found to be the measuring of the distances on the interferograms, which were unfortunately not very clear. There were 40 interferograms to be analyzed and a total of 3712 measurements to be made on those interferograms. Two techniques were tried to ease the problem but they failed. The first technique was the use of "densitometer" which is available in the Aero-Propulsion Laboratory of Wright-Patterson U.S. Air Force Base. The densitometer scans a negative film or a transparency for density variations with the help of a thin beam of light. The density distribution is automatically plotted on a graph with a magnified distance scale. The method did not work because if too thin a beam of light was used to scan the negative, then the densitometer provided so much detail of the density variations that it became impossible to find the center of a fringe. In the case of a thicker beam of light, the densitometer would not detect the clustered, thin fringes near the walls of the cavity. The second technique was to project an enlarged image of the negative on a screen and make the measurements with a scale. This technique gave very bad results and was also abandoned. The measurements were finally made with the help of a microcomparator.

IV. RESULTS

Interferograms

As mentioned earlier, in Section III, the study was carried out for five different aspect ratios. Each aspect ratio was studied at four different angles of inclination and two plate temperature differences. The results achieved from these studies are included in this section. Figures 10-15 include the interferograms for the different geometries at various angles. These interferograms are for the lower temperature difference between the plates. The rest of the interferograms are in the custody of the Department of Aeronautics and Astronautics at AFIT.

Figure 10 consists of the interferograms for the 5.93" x 0.525" geometry (Aspect Ratio = 11.295). Figure 10(a) shows the initial finite fringe pattern when there is no temperature difference between the vertical plates. The fringes have to be adjusted in a similar way, perpendicular to the plates, whenever a cavity is placed at a new angle. Figure 10(b) is the interferogram of the vertical, 5.93" x 0.525" geometry with a temperature difference between the plates of 24.6°F. It is clear from the interferogram that the fringes in the central part of the cavity are almost straight lines, indicating a linear temperature distribution between the plates. This means that in most of the central portion of the cavity, the mode of the heat transport is predominantly conduction.

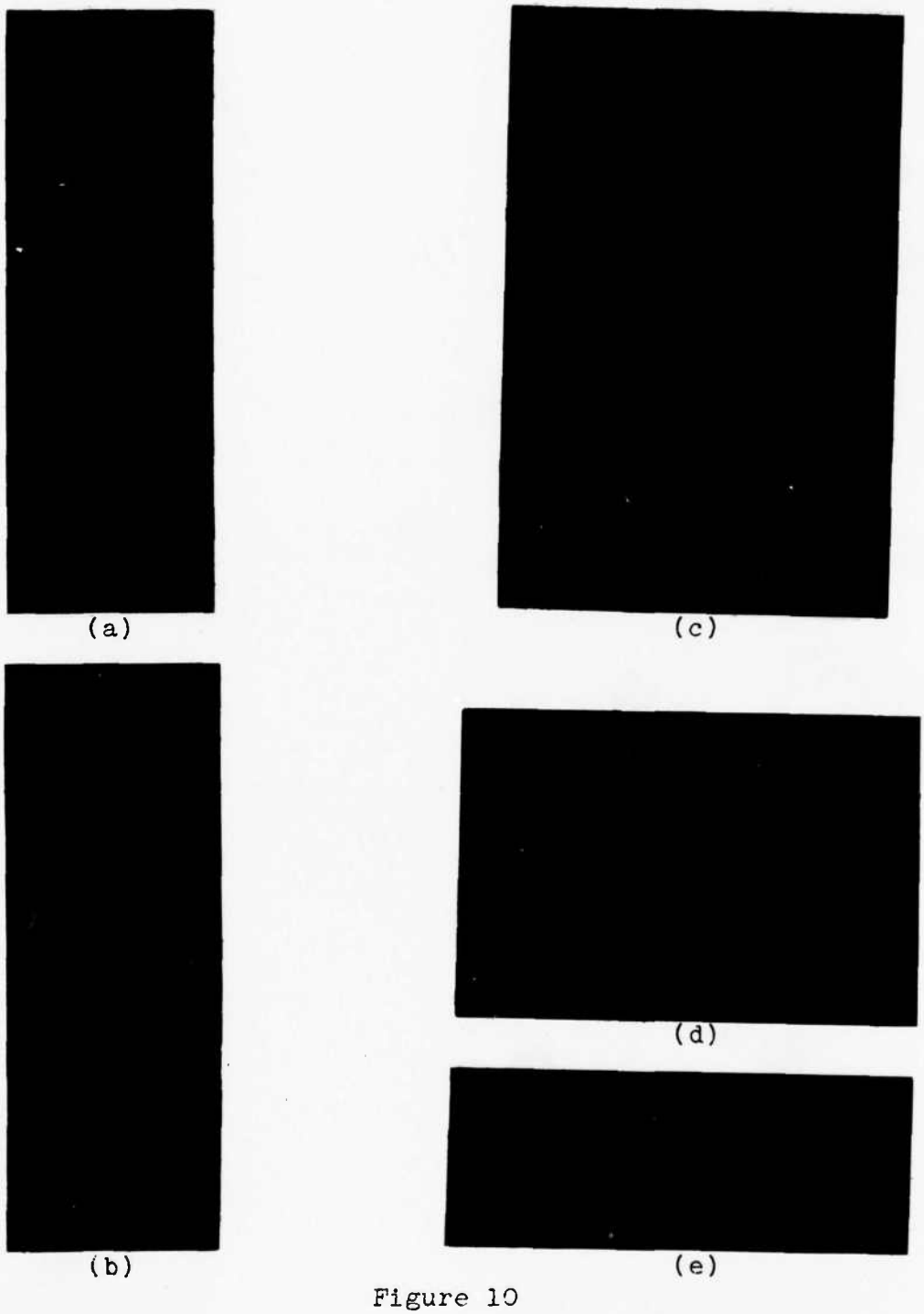

Figure 10

a) 5.93" x 0.525" at 90° and $\Delta T = 0$
b) 5.93" x 0.525" at 90° and $\Delta T = 24.575^{\circ}F$
c) 5.93" x 0.525" at 60° and $\Delta T = 23.213^{\circ}F$
d) 5.93" x 0.525" at 30° and $\Delta T = 26.151^{\circ}F$
e) 5.93" x 0.525" at 0° and $\Delta T = 19.347^{\circ}F$

Some convective heat transport is taking place at both ends of the cavity. The fringes are close-together near the bottom of the hot plate and the top of the cold plate, indicating the presence of boundary layers. The fluid flow pattern can be pictured as one large cell with the fluid rising near the hot plate, falling near the cold plate. Because the two plate boundary layers interfer, the streamlines are nearly parallel to the bounding surfaces everywhere except at the extreme ends of the cavity where the fluid turns. Thus, the heat transfer is mostly conductive except at the ends.

Figures 10(c), (d), and (e) are the interferograms of the same geometry (5.93" x 0.525") at 60^{o}, 30^{o}, and 0^{o} angles of inclination. All of these interferograms can be seen only partially. To find the average heat flux over any of the plates, it is necessary that the distribution of local heat fluxes be known over the entire plate. To overcome this problem, it has been assumed that the local heat flux distribution over the top half of the hot plate is equivalent to that on the lower half of the cold plate. This assumption has been found to be valid by previous studies and to some extent by the present study for all the geometries at 90^{o}, when the whole cavity is visible on the interferograms. It is clear from Figure 10(c) that the mode of the heat transport over most of the central part of the cavity is still conduction. Figures 10(d) and (e) show that convection is the predominant

means of heat transport over the entire cavity, even though the ΔT for the 0^{o}-case (Figure 10(e)) is only $19.347^{o}F$ as compared to $24.575^{o}F$ of the 90^{o}-case (Figure 10(b)).

Figure 11 consists of the interferograms of 2.786" x 3.00" geometry (Aspect Ratio = 0.929). It is clear from the interferograms that in all of the cases, it is convection which is the predominant mode of heat transfer. It can also be observed that in all the cases, except when the cavity is at 0^{o} (Figure 11(d)), the fringes are very close together near the bottom of the hot plate, and they separate upwards along the hot plate. The same phenomenon can be observed along the cold plate also, but in the opposite direction. This shows that a boundary layer is formed on both the plates, which is the thinnest at the bottom of the hot plate and the top of the cold plate. It can also be observed from all the interferograms that the fringes in the core-region between the two boundary layers are almost perpendicular to the plates, thus having very little displacement from their initial position. This means that there is very little conduction in the core-region. Since the heat flux is concentrated in the boundary layer regions and the boundary layers are the thinnest at the bottom of the hot plate and the top of the cold plate, it can be predicted from the interferograms that the rate of heat flux will be very high near the bottom of the hot plate and the top of the cold plate. There is some strange phenomenon occurring in the top corner of the

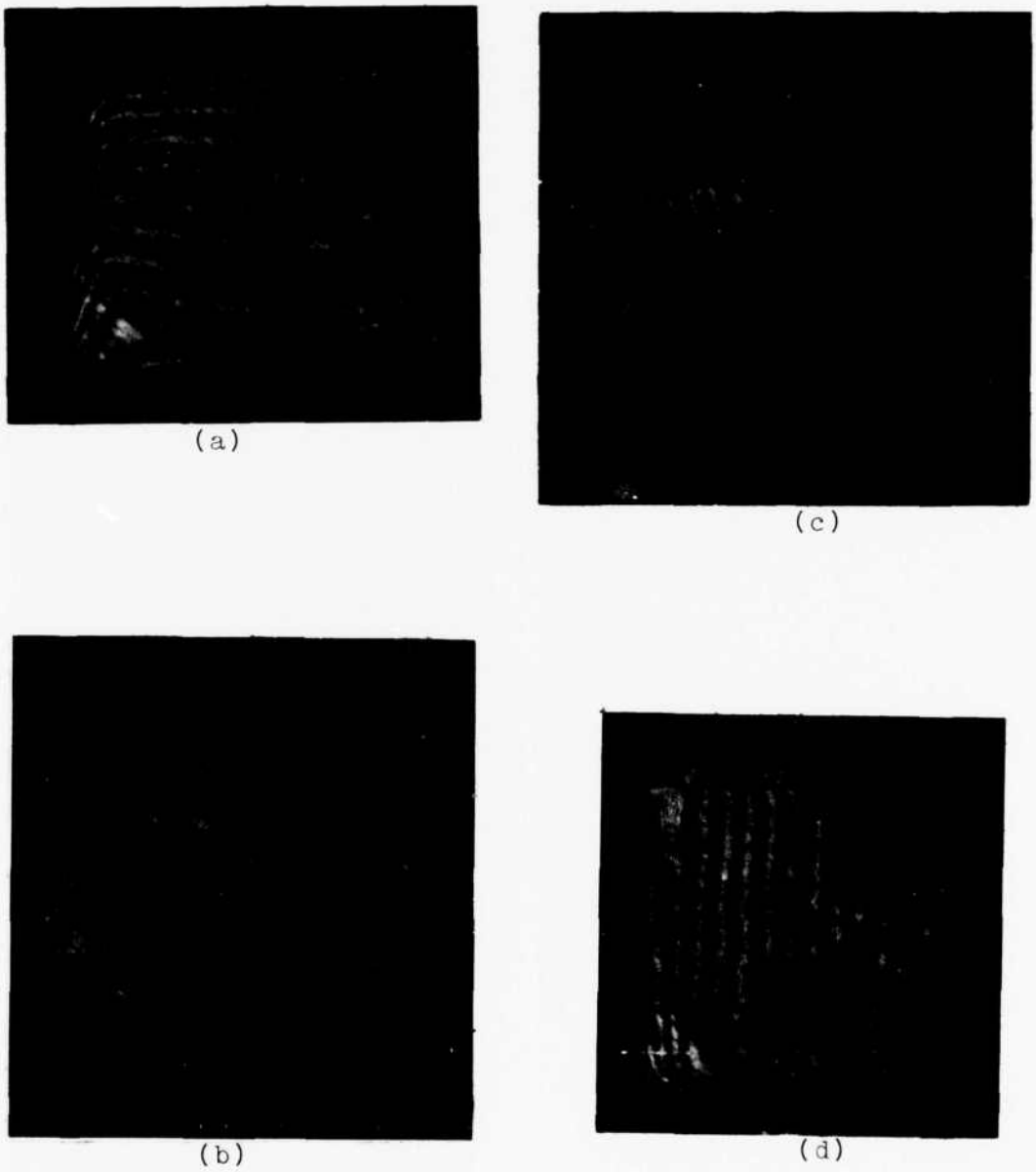

Figure 11

a) 2.786" x 3.0" at 90° and $\Delta T = 24.183^{\circ}F$
b) 2.786" x 3.0" at 60° and $\Delta T = 26.375^{\circ}F$
c) 2.786" x 3.0" at 30° and $\Delta T = 39.753^{\circ}F$
d) 2.786" x 3.0" at 0° and $\Delta T = 25.00^{\circ}F$

core-region, near the hot plate, and in the bottom corner of the core-region, near the cold plate, which is as yet unexplained. It can be observed from Figure 11(d) that in the 0^{o}-case, the boundary layers seem to be of almost uniform thickness over the plates. These are essentially stagnant conduction layers separated by the core-region where energy is transported by convection.

Figure 12(a) consists of a 2.786" x 3.00" geometry placed at 90^{o} but with a diagonal partition inserted into the cavity. The partition was made of 0.1" thick hard cardboard with both sides covered with white paper. The partition was placed in such a way that the hot plate remained below it. By the insertion of the partition, two new boundary layers have been introduced into the flow, one along each surface of the partition. The triangular cavities formed by the partition have more stagnant areas in the corners, resulting in less convection. Both of these effects decrease the heat flux between the plates.

Figure 12(b) is the interferogram for 5.9" x 3.0" geometry placed at 90^{o} and with a $\Delta T = 22.51^{o}F$. It is clearly noticeable that the fringe pattern seems to be similar to that of a 2.786" x 3.00" geometry; therefore, the rest of the interferograms have not been exhibited in the report.

Figure 13 consists of the interferograms of 5.9" x 1.5" geometry for all four angles. One can notice from these pictures that the flow is definitely of the boundary

(a)

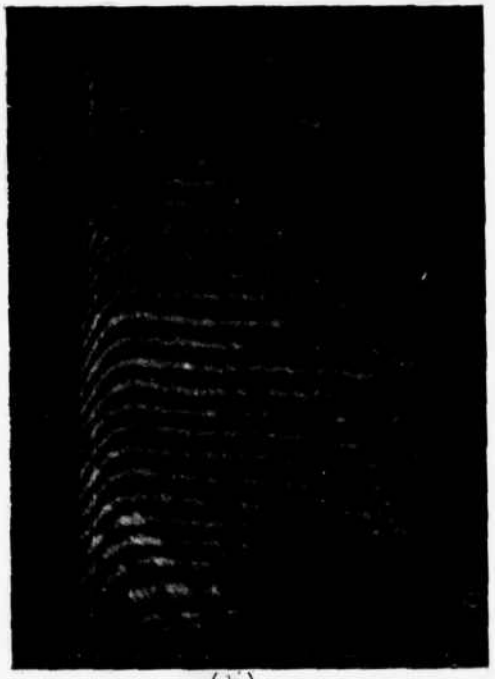

(b)

Figure 12

a) 2.786" x 3.0" at 90° with diagonal partition and with $\Delta T = 39.355^{\circ}F$
b) 5.9" x 3.0" at 90° and with $\Delta T = 22.51^{\circ}F$

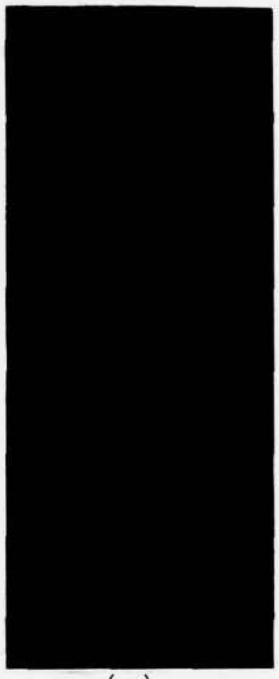

(a)

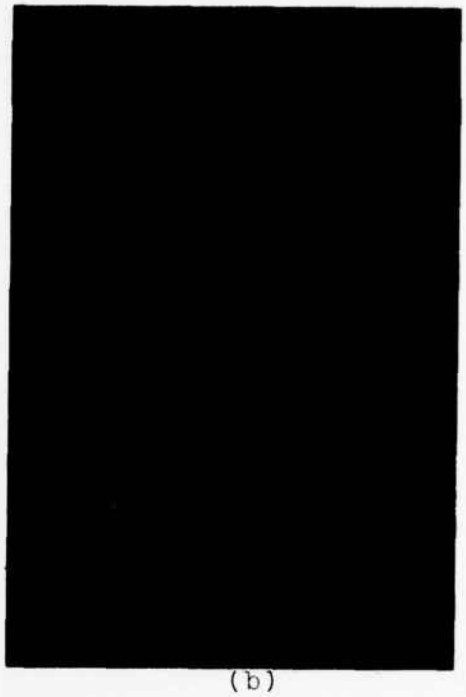

(b)

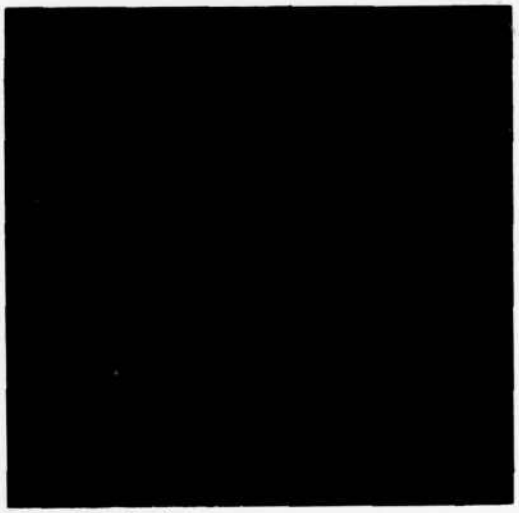

(c)

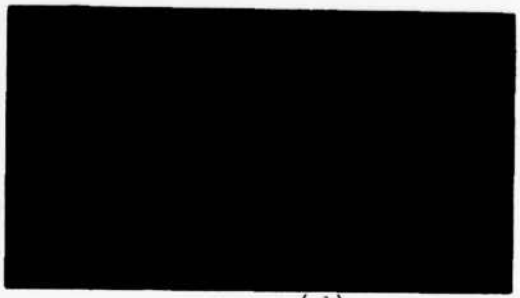

(d)

Figure 13

a) 5.9" x 1.5" at 90° with $\Delta T = 25.788^{\circ}F$
b) 5.9" x 1.5" at 60° with $\Delta T = 20.522^{\circ}F$
c) 5.9" x 1.5" at 30° with $\Delta T = 13.435^{\circ}F$
d) 5.9" x 1.5" at 0° with $\Delta T = 21.818^{\circ}F$

layer type. It can also be noticed that the deflection of the fringes in the core-region becomes less as one decreases the angle of inclination from 90^{o} to 0^{o}. It can probably be deduced that the core becomes more and more isothermal as one decreases the angle of inclination of the cavity.

Figure 14(a) is the interferogram of 5.9" x 0.75" geometry at 90^{o} and with $\Delta T = 19.348^{o}F$, while Figure 14(b) is the interferogram of the same geometry at the same angle but with $\Delta T = 33.818^{o}F$. The fringes become more slanted and closer together as the temperature difference between the plates, ΔT, is increased. Both of the effects, of course, mean higher heat flux. Figures 14(c) and (d) are the interferograms at two different ΔTs for the 60^{o}-case of the same geometry. These two pictures show the same effects of a higher ΔT. It can be noticed from Figures 14(a) and (c), the lower ΔT cases for both the angles, that the fringes in the central protion of the cavity can be approximated as straight lines, thus showing that conduction may be a significant part of the heat transfer. While there seems to be almost no core region for the lower ΔT cases of both the angles, there is a definite core-region, which is almost isothermal for the higher ΔT cases. Figure 15 consists of interferograms of the same geometry at 30^{o} and 0^{o} with lower and higher ΔT. These interferograms show that the flow is boundary layer type for all of the cases, and convection is the predominant

means of heat transport in the core-region, even for the lower ΔT cases.

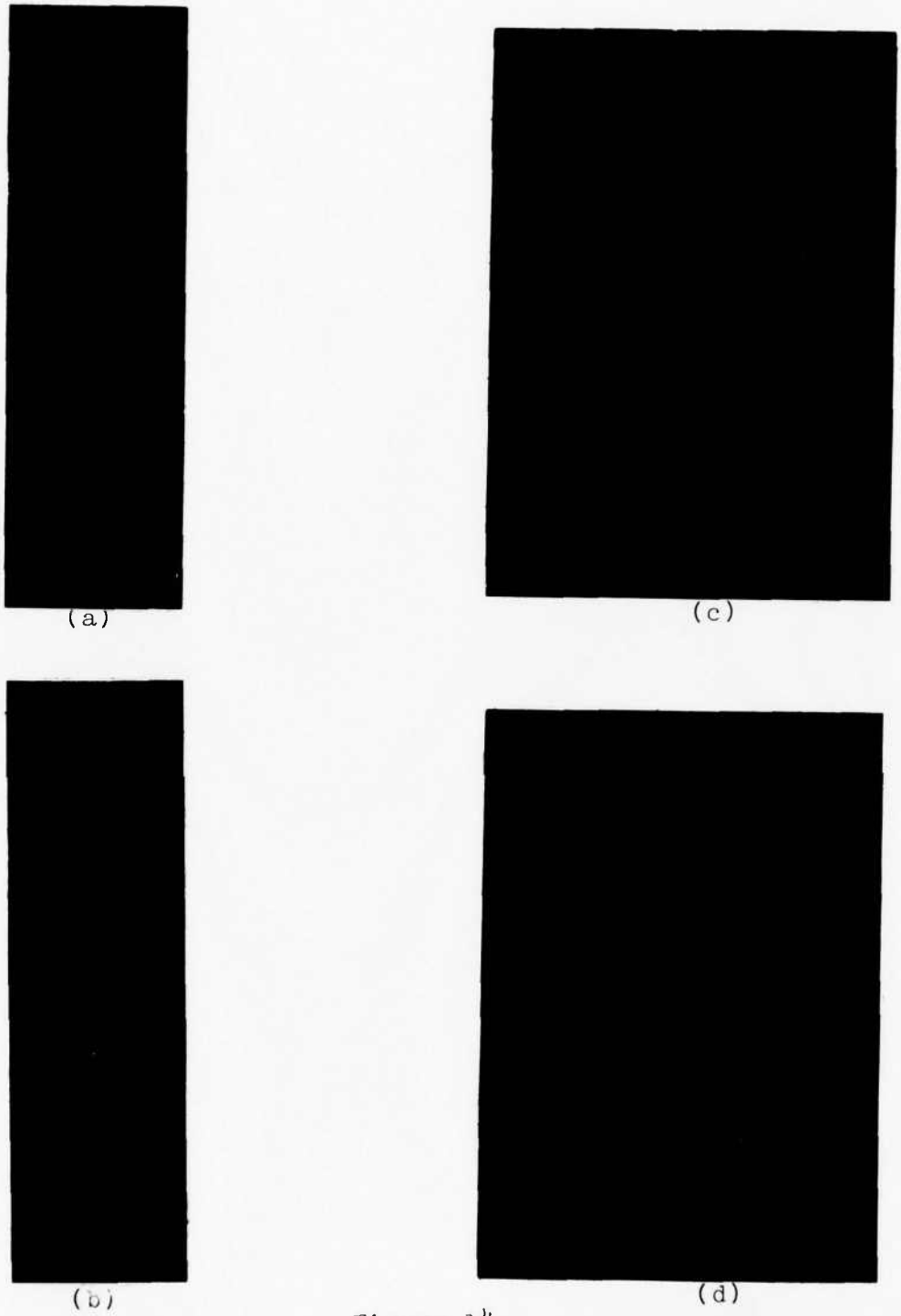

Figure 14

a) 5.9" x 0.75" at 90° with $\Delta T = 19.348^{\circ}F$
b) 5.9" x 0.75" at 90° with $\Delta T = 33.818^{\circ}F$
c) 5.9" x 0.75" at 60° with $\Delta T = 21.962^{\circ}F$
d) 5.9" x 0.75" at 60° with $\Delta T = 37.435^{\circ}F$

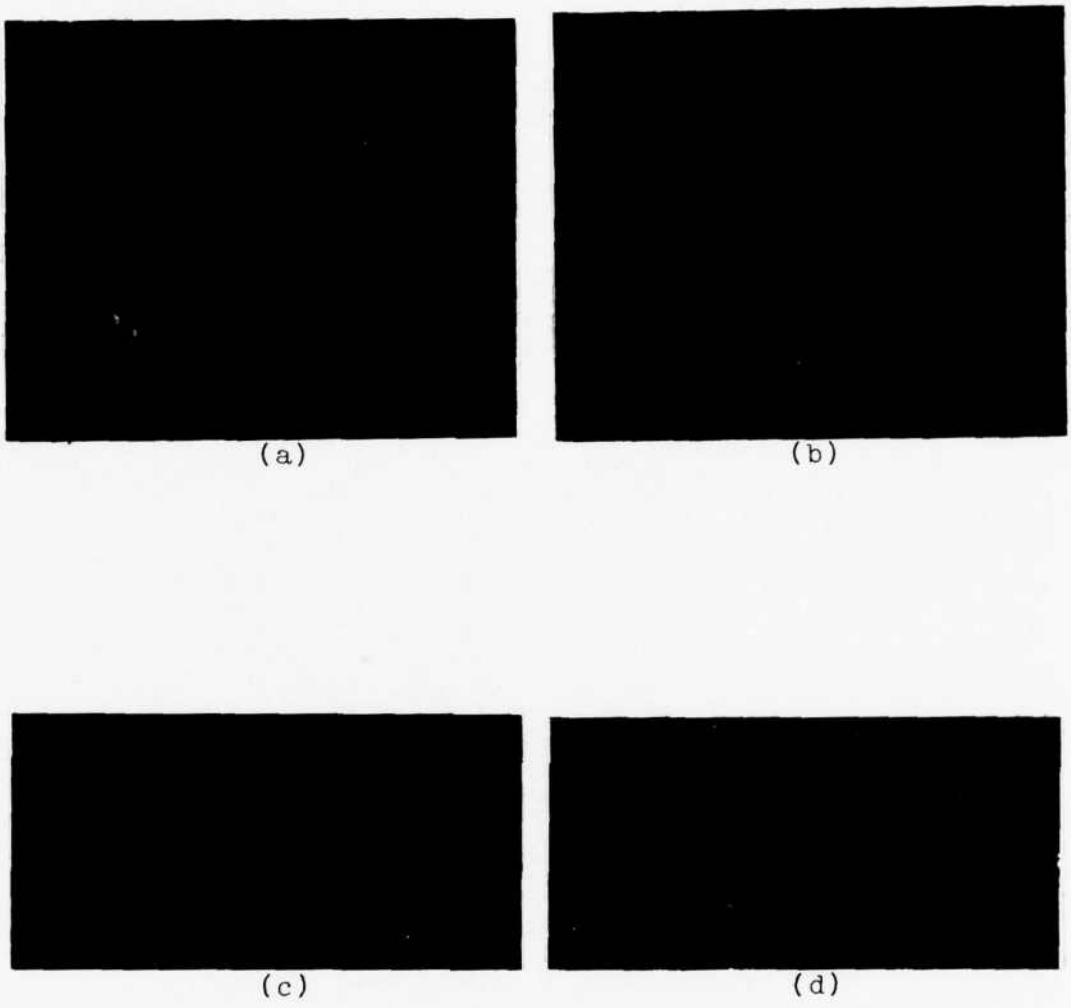

Figure 15

a) 5.9" x 0.75" at 30° with $\Delta T = 23.803^{\circ}F$
b) 5.9" x 0.75" at 30° with $\Delta T = 41.608^{\circ}F$
c) 5.9" x 0.75" at 0° with $\Delta T = 18.863^{\circ}F$
d) 5.9" x 0.75" at 0° with $\Delta T = 38.304^{\circ}F$

Local Heat Flux

Local heat fluxes were calculated at twenty positions along the hot plate and the cold plate for the geometries having a height of 5.9" and at eight positions for the 2.786" x 3.00" geometry. These positions are equally spaced and are numbered starting from the bottom of the plate. Local heat fluxes for two vertical geometries are presented in Tables I and II. The rest of the local heat flux data is provided in Appendix C.

Table I

Local Heat Fluxes for 5.93" x 0.525" Geometry
Aspect Ratio = 11.295, $\Delta T = 24.575^{o}F$, $\phi = 90^{o}$

Position Number	Distance Along the plate "x" (in)	Local Heat Fluxes at Hot Plate (Btu/hr ft²)	Local Heat Fluxes at Cold Plate (Btu/hr ft²)
1	0.0	10.3	- 3.9
2	0.324	26.9	- 3.8
3	0.648	20.6	- 6.2
4	0.972	16.5	- 7.4
5	1.296	13.8	- 9.4
6	1.620	12.9	- 7.3
7	1.945	9.7	- 9.8
8	2.227	10.1	-10.2
9	2.593	10.2	-10.1
10	2.917	10.1	-10.3
11	3.014	10.6	- 9.8
12	3.338	9.9	-10.0
13	3.662	9.2	- 9.9
14	3.086	9.6	-10.0
15	4.310	7.4	-13.2
16	4.634	9.0	-13.9
17	4.958	7.3	-16.1
18	5.283	6.6	-21.3
19	5.607	4.2	-28.5
20	5.930	4.3	-10.1

Average Heat Flux at the Hot Plate = 11.17 $\frac{\text{Btu}}{\text{hr ft}^2}$

Average Heat Flux at the Cold Plate = 11.33 $\frac{\text{Btu}}{\text{hr ft}^2}$

Table II

Local Heat Fluxes for 2.786" x 3.00" Geometry
Aspect Ratio = 0.929, ΔT = 24.183°F, ϕ = 90°

Position Number	Distance Along the plate "x" (in)	Local Heat Fluxes at Hot Plate (Btu/hr ft²)	Local Heat Fluxes at Cold Plate (Btu/hr ft²)
1	0.0	3.1	- 3.8
2	0.398	18.4	- 4.2
3	0.796	15.4	- 8.8
4	1.194	9.9	- 9.4
5	1.592	9.6	-12.8
6	1.990	6.4	-17.5
7	2.388	5.1	-19.6
8	2.786	5.3	- 3.4

Average Heat Flux at the Hot Plate = 9.87 $\frac{\text{Btu}}{\text{hr ft}^2}$

Average Heat Flux at the Cold Plate = 10.72 $\frac{\text{Btu}}{\text{hr ft}^2}$

The local heat flux data of the two geometries has been presented here to show that the local heat fluxes on correspondingly opposite positions of the two plates are at least similar, if not nearly equal. The percentage difference of the local heat fluxes of position 1 of the hot plate and position 20 of the cold plate of the 5.93" x 0.525" geometry (see Table I), for example, is only 2.05%. The main concern is about the equality of the local heat

fluxes on correspondingly opposite positions at the top of the hot plate and the bottom of the cold plate, because in any inclined geometry the local heat fluxes on the top half of the hot plate have been substituted for the local heat fluxes on the lower half of the cold plate. This was, of course, not necessary for the 2.786" x 3.00" geometry, because that particular geometry was completely visible in the interferogram. It can be noticed from Table I that for the 5.93" x 0.525" geometry the difference between the local heat fluxes at position 20 (top) of hot plate and position 1 (bottom) of the cold plate is 11.5%. The difference for the same two corners for the second case (see Table II) is 31.54% which is much larger than the other value. Figure 16 shows the temperature distributions for a 2.786" x 3.00" geometry, placed at 90^{o} and with a $T = 38.749^{o}F$. It is clear that the slope of the temperature profile at the top of the hot plate is more than the slope at the bottom of the cold plate, indicating that the local heat flux at the top of the hot plate is higher than the heat flux at the bottom of the cold plate. It can also be noticed from Tables I and II that there is a lot of scatter in the data of local heat fluxes. These differences are most probably due to random errors in measuring the distances on an interferogram. Significant errors are also introduced while calculating the temperature gradients, numerically. In addition, complex radiative effects may also cause some difference between the local heat fluxes

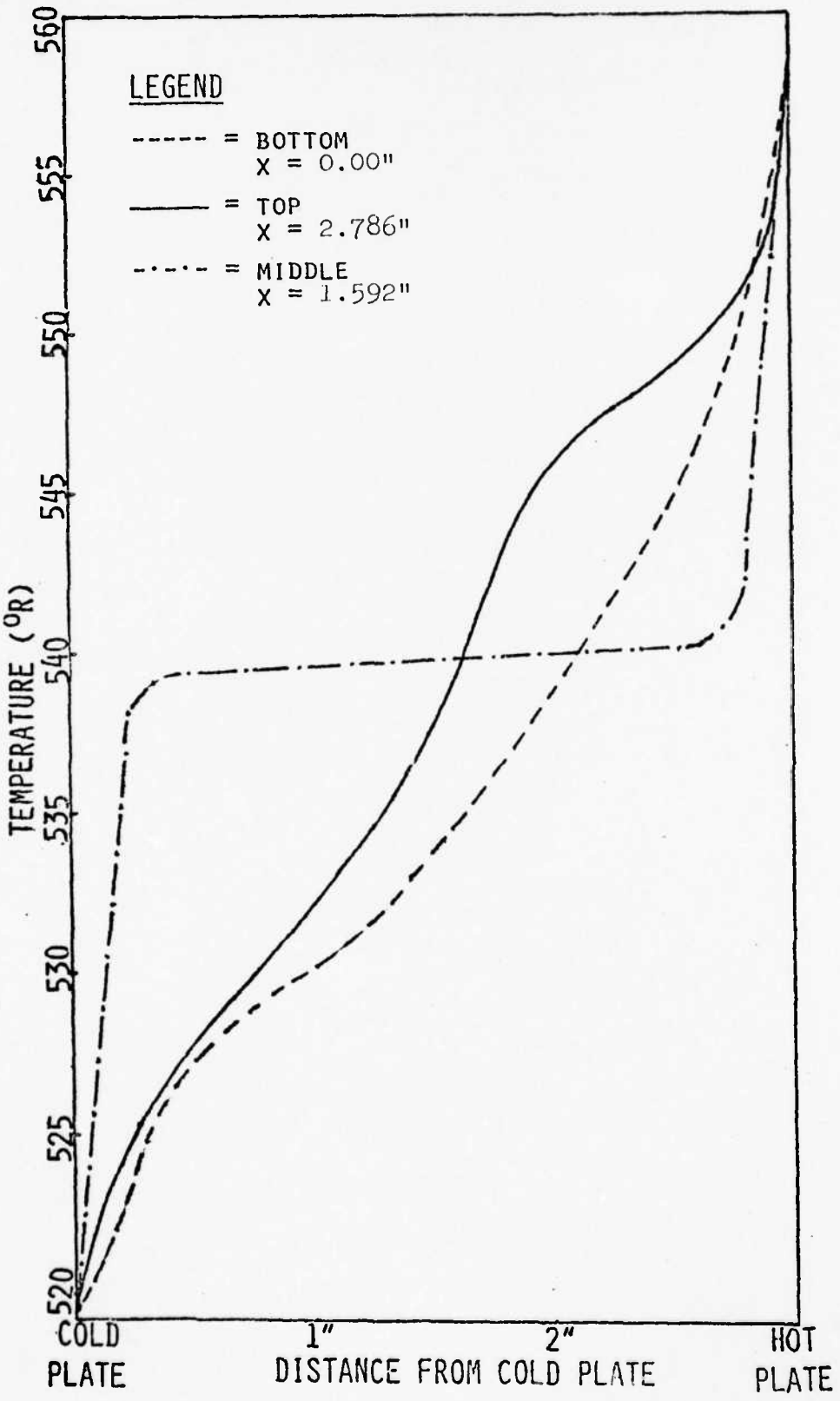

Figure 16. End Wall Temperature Distributions for a 2.786" x 3.00" Geometry at 90° and $\Delta T = 38.744^{\circ}F$.

at the top of the hot plate and the bottom of the cold plate. Nevertheless, the local heat fluxes at the top of the hot plate constitute a small part of the total heat flux from the hot plate, so the error introduced by replacing these be the local heat fluxes at the bottom of the cold plate is not too high.

Figures 17-19 show the distribution of local Nusselt numbers on the hot plate for 5.9" x 0.75" geometry (Aspect Ratio = 7.867) for 90^{o}, 60^{o}, and 30^{o} angles of inclination, respectively.

$$\text{Local Nusselt Number} = \frac{q*L}{T*k}$$

where q = local heat flux (Btu/hr ft)

L = thickness of air layer (ft)

T = temperature difference between the plates (^{o}F)

k = thermal conductivity of air (Btu/hr ft ^{o}F)

It can be observed from Figures 17-19 that the heat flux at the very bottom of the hot plate is low and it rises immediately to a peak value as one moves a small distance up the hot plate. The low value of the heat flux at the very bottom of the hot plate is due to a stagnant region in the corner of the cavity. The heat flux rises to a high value as one goes out of this stagnant region, because at the bottom of the hot plate the boundary layer is very thin. The local heat flux then keeps decreasing as one moves up the hot plate because the boundary layer develops

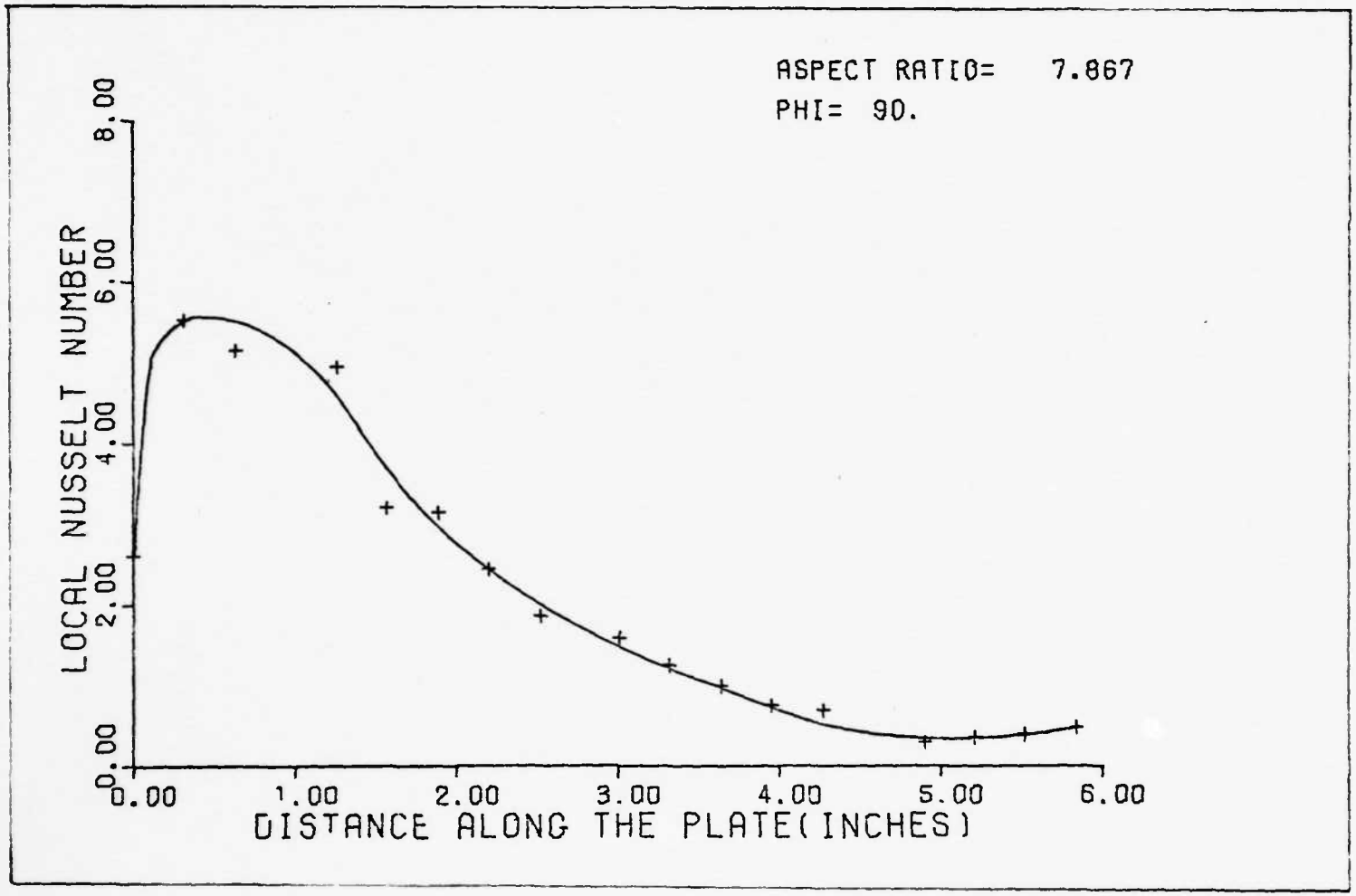

Figure 17 . Distribution of local Nusselt number on the hot plate for 5.9" x 0.75"

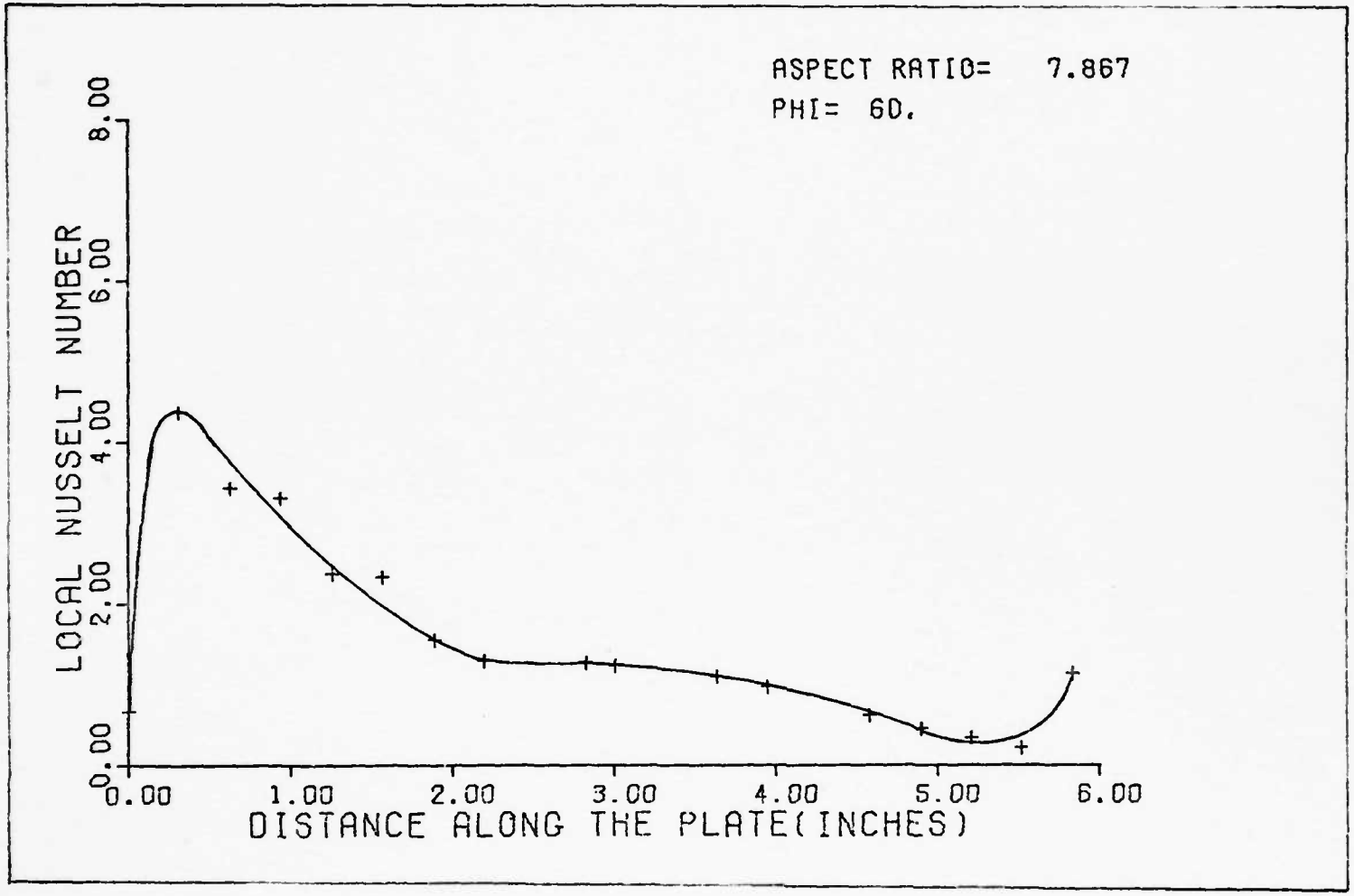

Figure 18 . Distribution of local Nusselt number on the hot plate for 5.9" x 0.75"

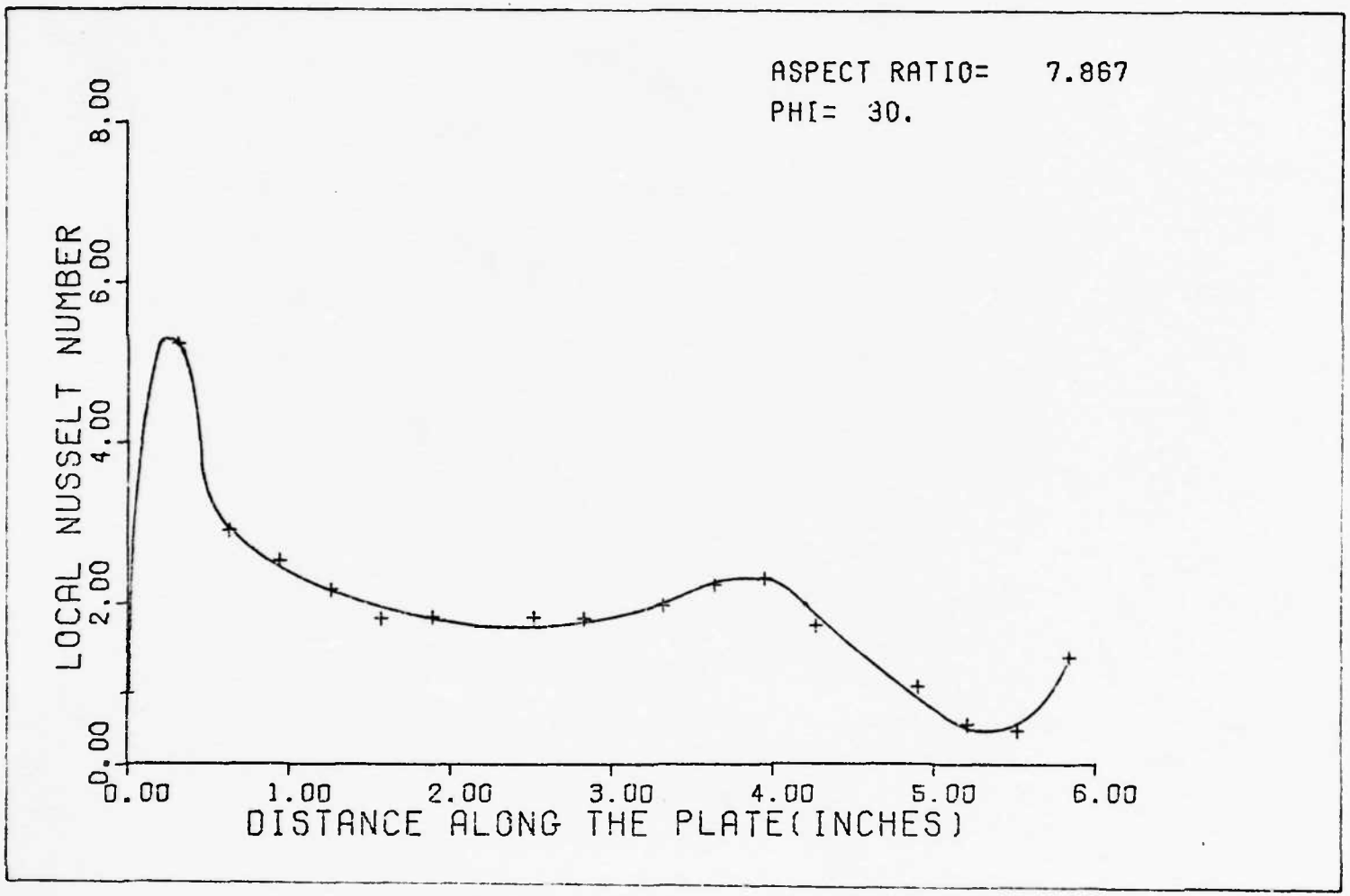

Figure. 19 . Distribution of local Nusselt number on the hot plate for 5.9″ x 0.75″

and becomes thicker. It can be observed from these plots that as the angle of inclination is changed from 90^{o} to 60^{o} and then to 30^{o}, the heat flux drops off more steeply after reaching a peak value, as one moves up the hot plate. After the drop, the heat flux becomes more uniform along the hot plate. The reason is that the buoyant force, which always works in the vertical direction against gravity, has a component perpendicular to the plate when the angle of inclination is any other than 90^{o}. This component of the buoyant force pulls the air in the boundary layer away from the plate, thus thickening the boundary layer, faster. As the angle of inclination is decreased further, this effect increases and the boundary layer develops even faster. The faster the development of the boundary layer, the steeper would be the drop in the local heat flux. As the boundary layers on the hot and the cold plates grow faster, they soon join each other and the heat flux becomes almost uniform over both the plates.

Figure 20 is the local Nusselt number distribution on the hot plate for 5.9" x 0.75" geometry (Aspect Ratio = 7.867) at 0^{o}. It can be observed from this plot that the heat flux is low at the very bottom of the hot plate due to the stagnant region, it rises to a high value as one goes up the hot plate, remains almost uniform over most of the plate and then drops down as one approaches the stagnant region at the top of the plate. The exact nature of the flow in a horizontal cavity is quite complex. It is quite

evident from the interferograms and Figure 20 that there is almost uniform heat flux over the plates and most of the temperature change takes place in a thin layer near the plates, while the core is almost isothermal. Figure 21 is the local Nusselt number distribution over the cold plate for the same geometry at 90^{o}. As can be seen, it is exactly opposite to Figure 17.

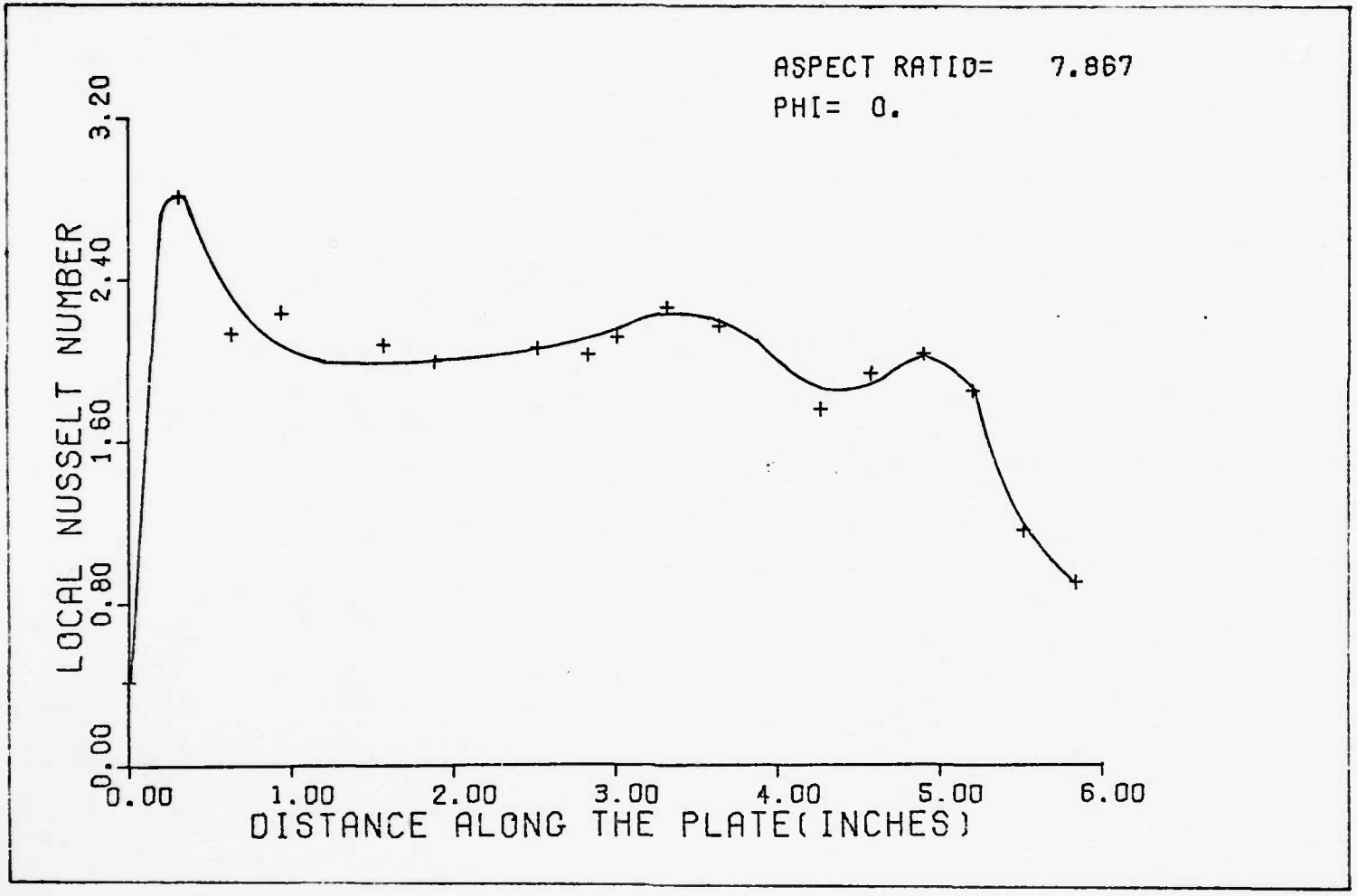

Figure 20 . Distribution of local Nusselt number on the hot plate for 5.9″ x 0.75″

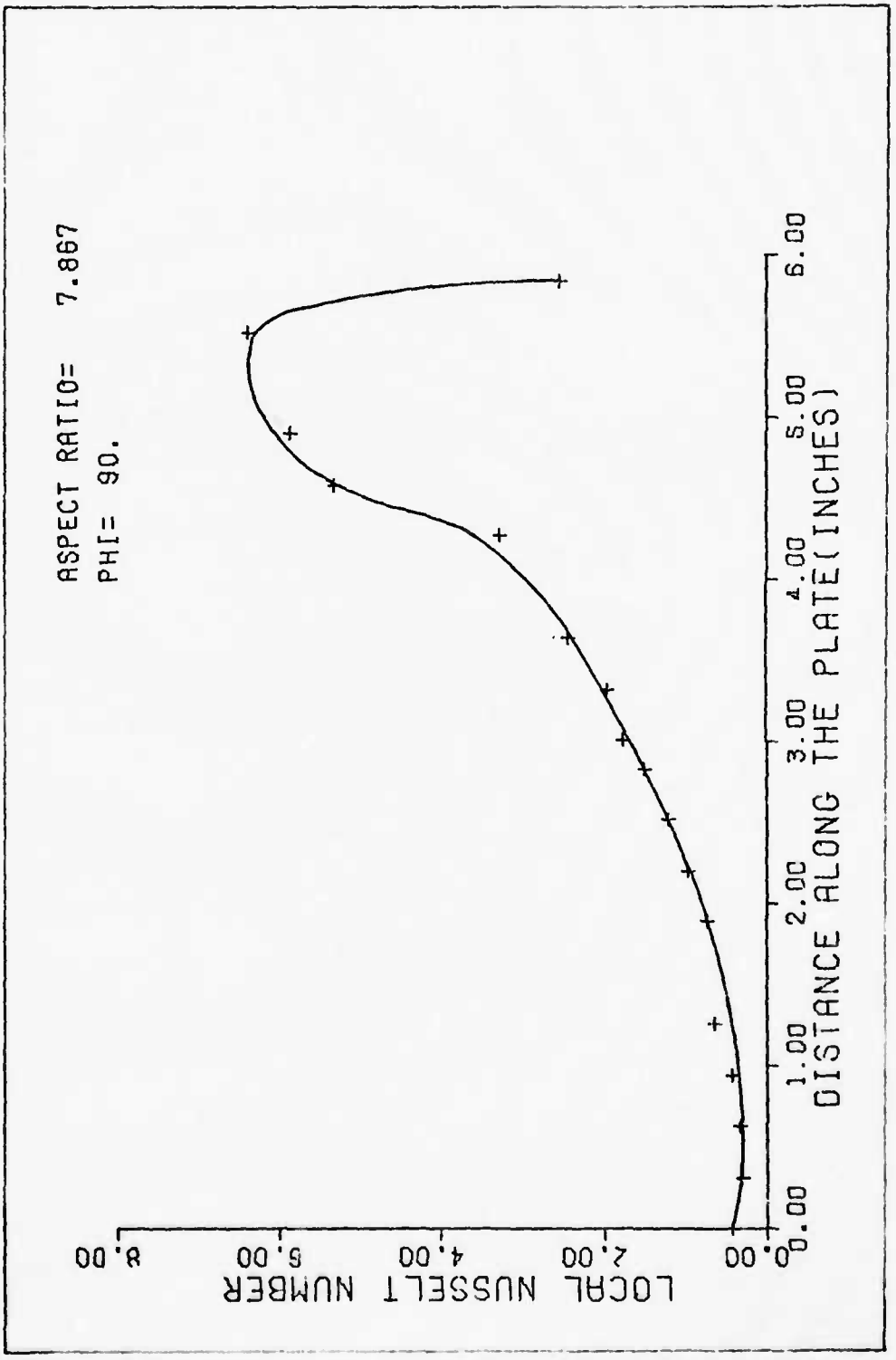

Figure 21 . Distribution of local Nusselt number on the cold plate for 5.9" x 0.75".

Average Heat Flux

The average heat fluxes are provided in Tables III - VII in the form of average Nusselt numbers, $\overline{Nu}$, where the average Nusselt number $\overline{Nu}$ is based on L, the width of the air layer. The average Nusselt numbers have been presented against either Grashof numbers in the case of 90^{o} inclination (Tables III and IV) or Rayleigh numbers in the case of 60^{o}, 30^{o} and 0^{o} inclinations (Tables V, VI, and VII). Both the Grashof numbers and the Rayleigh numbers are based on L, the width of the air layer. The theoretical Nusselt numbers given in Table III, which consists of low Grashof numbers (conductive regime), were calculated by the empirical equation (1).

$$\overline{Nu} = 1 + 0.00166 \frac{L}{H} (Gr)^{0.9} \qquad (1)$$

Table IV, which consists of high Grashof numbers (boundary layer regime), provides theoretical Nusselt numbers which were calculated by the empirical equation (2).

$$\overline{Nu} = 0.119 (Gr)^{0.3} (\frac{L}{H})^{0.1} \qquad (2)$$

Equations (1) and (2) were extracted from Reference 8. The theoretical Nusselt numbers provided in Tables V - VII were calculated by the empirical equation (3).

$$\overline{Nu} = 1 + 1.44 \left[1 - \frac{1708}{Ra \cos \phi}\right]^{\cdot} \left(1 - \frac{(\sin 1.8\phi)^{1.6}\ 1708}{Ra \cos \phi}\right) + \left(\frac{Ra \cos \phi}{5830}\right)^{1/3} - 1\Big]^{\cdot} \qquad (3)$$

where $[\,]^{\cdot}$ is defined by:

$$[x]^{\bullet} = (|x| + x)/2$$

Equation (3) was extracted from Reference 6.

Table III

Average Nusselt Numbers for
Low Grashof Numbers, $\phi = 90^{o}$

Grashof Number	$\overline{Nu}$ (Experimental)	$\overline{Nu}$ (Theoretical)	% Difference
4613.07	1.34	1.29	3.8
6229.54	1.27	1.38	8.3
17497.02	2.21	2.39	7.8

Table IV

Average Nusselt Numbers for
High Grashof Numbers, $\phi = 90^{o}$

Grashof Number	$\overline{Nu}$ (Experimental)	$\overline{Nu}$ (Theoretical)	% Difference
107662.20	3.34	3.36	0.6
152281.42	3.90	3.73	5.2
766760.97	6.63	6.48	2.3
843023.22	7.14	7.19	0.7
1244511.49	7.83	7.49	4.4
1287084.44	8.68	8.16	6.2

Table V

Average Nusselt Numbers for $\phi = 60^{\circ}$

Rayleigh Number	$\overline{Nu}$ (Experimental)	$\overline{Nu}$ (Theoretical)	% Difference
2994.1	0.99	1.00	1.0
4386.4	1.22	1.09	11.2
8403.7	1.51	1.53	1.3
13563.2	1.70	1.88	10.1
62647.2	2.74	3.04	10.4
111669.0	3.55	3.48	2.0
455359.8	5.27	4.81	9.1
630896.8	5.57	5.21	6.7
1099864.0	5.74	5.98	4.2

Table VI

Average Nusselt Numbers for $\phi = 30^{\circ}$

Rayleigh Number	$\overline{Nu}$ (Experimental)	$\overline{Nu}$ (Theoretical)	% Difference
3496.3	1.23	1.37	10.8
4963.1	1.50	1.62	7.7
9016.9	1.90	2.05	7.6
43454.9	3.12	3.19	2.2
113075.0	3.46	3.96	13.5
605935.5	6.44	5.91	8.6
877750.9	6.08	6.51	6.8
1150561.1	6.89	6.99	1.4

Table VII

Average Nusselt Numbers for $\phi = 0^{\circ}$

Rayleigh Number	$\overline{Nu}$ (Experimental)	$\overline{Nu}$ (Theoretical)	% Difference
2587.3	1.47	1.49	1.4
4746.8	1.95	1.92	1.6
7201.0	1.95	2.17	10.7
67578.2	3.30	3.67	10.6
560077.7	6.44	6.02	6.7
609960.7	6.60	6.15	7.1
829539.9	6.16	6.66	7.8
936604.7	6.74	6.87	1.9

The results presented in Tables III - VII are given in Figures 22-26, respectively. Experimental and theoretical Nusselt numbers are plotted against Grashof numbers in the case of 90° (Figures 22 and 23), and these have been plotted against Rayleigh number x cos ϕ for 60°, 30°, and 0° angles of inclinations. It can be seen that the three empirical equations are within 11% difference from the experimental results. Considering the random errors in the experimental results, this error can be accepted and the empirical equations can be expected to give good results for Grashof numbers up to 1 million.

Figure 27 shows the dependence of average Nusselt number on the angle of inclination, ϕ, for a Grashof number of 200,000 and Aspect Ratio of 3.933 (5.9" x 1.5" geometry). The Nusselt number does not vary much as the angle of inclination, ϕ, is reduced from 90° to 60°. However, there is a

definite rise of about 12% in the Nusselt number as ϕ is reduced from 60^{o} to 30^{o}, and there is again very little change as ϕ is further reduced from 30^{o} to 0^{o}. Probably the flow mechanism in the cavity does not alter much if the angle of inclination of the cavity is changed from 90^{o} to 60^{o}. There seems to be a transition from the boundary layer type flow of the vertical geometry to the local cells type flow of the horizontal geometry, as the angle of inclination is reduced from 60^{o} to 30^{o}. The changes in the flow seem to be not much again, if the angle of inclination is further reduced from 30^{o} to 0^{o}. It can be, however, noticed that changes in the angle of inclination of an average aspect ratio geometry do not bring about drastic changes in the average Nusselt number, if the Grashof number is kept constant.

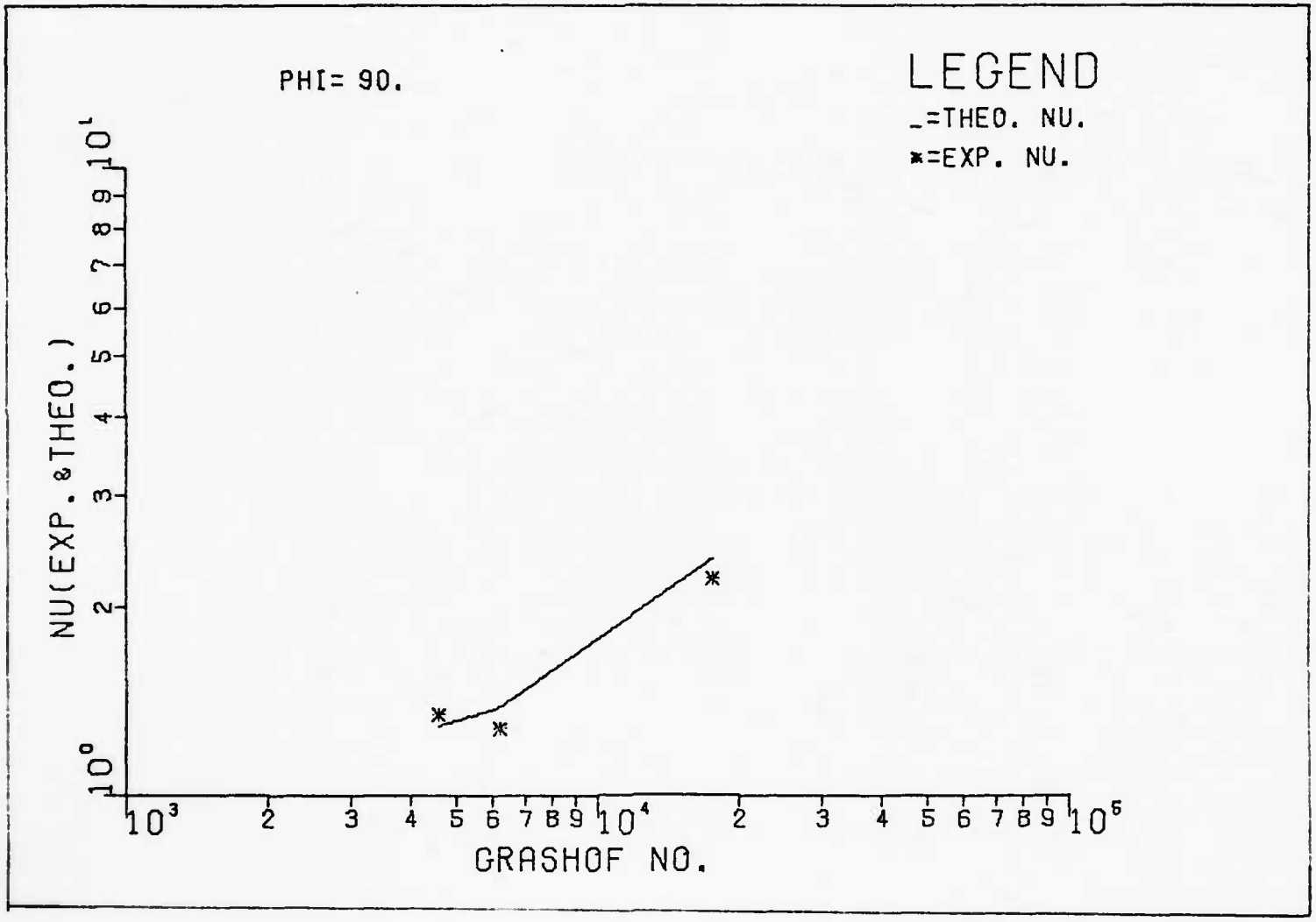

Figure 22 . A plot of theoretical and experimental Nusselt numbers vs Grashof numbers for low Grashof numbers.

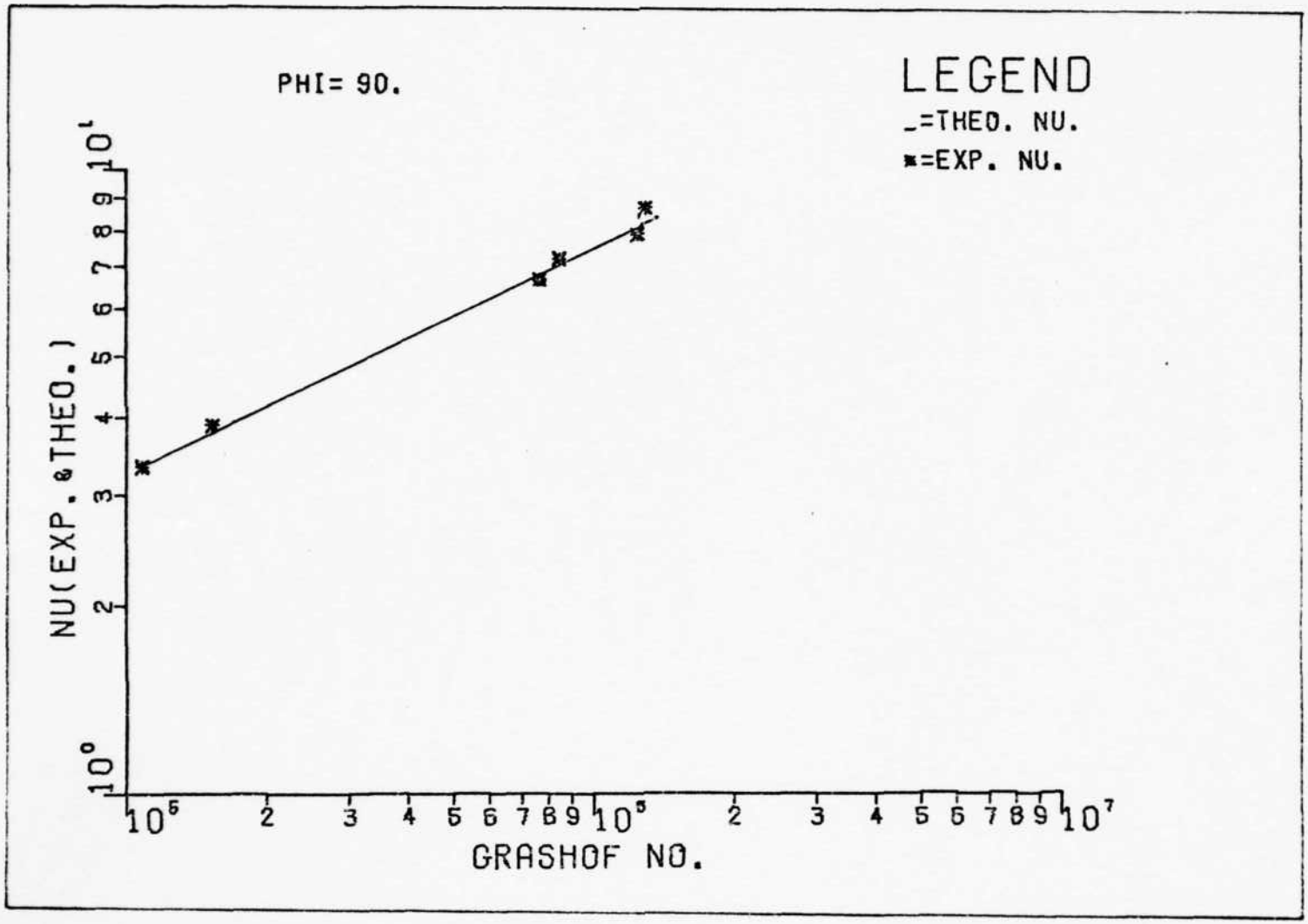

Figure 23. A plot of theoretical and experimental Nusselt numbers vs Grashof numbers for high Grashof numbers.

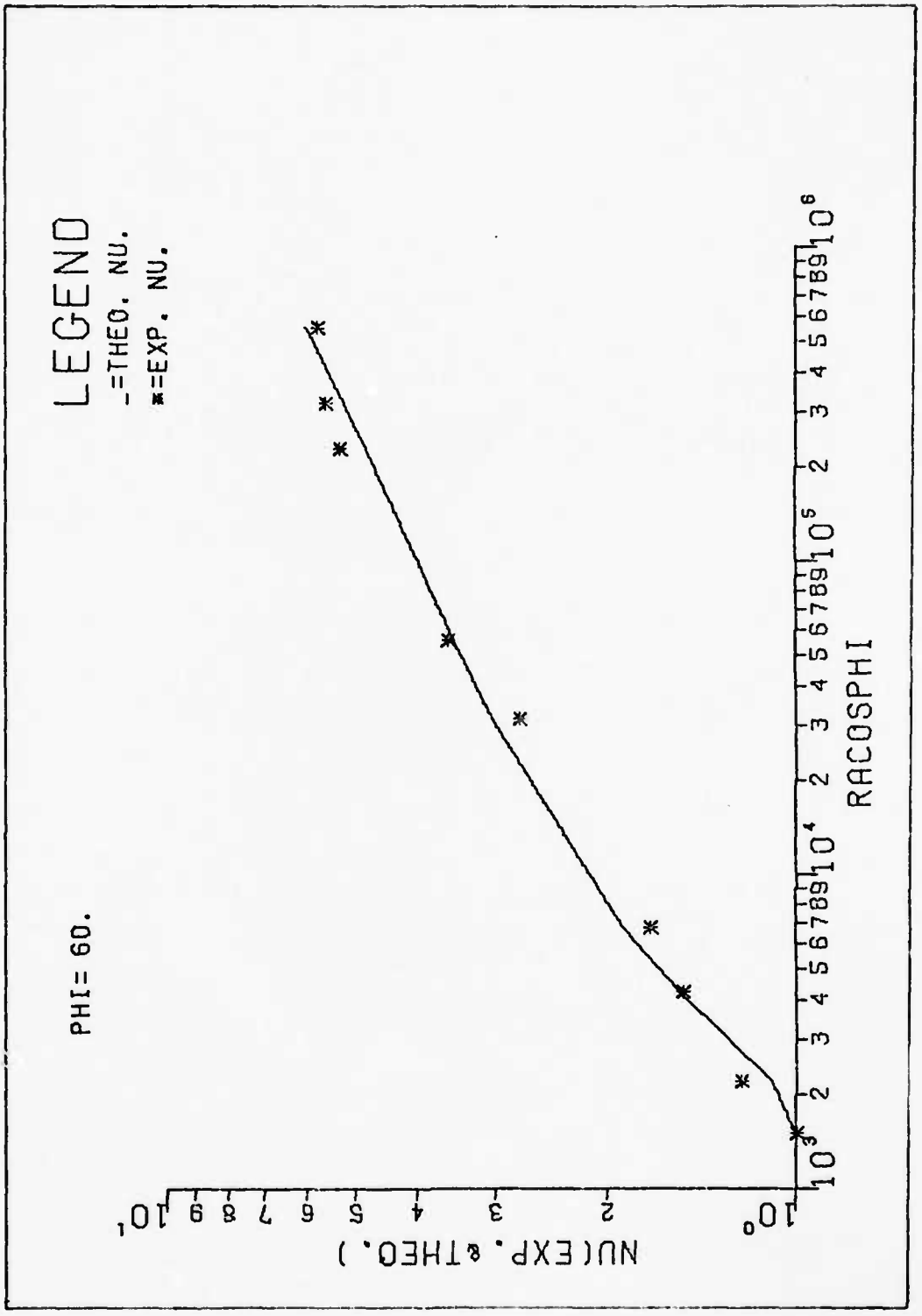

Figure 24 . A plot of theoretical and experimental Nusselt numbers vs (Rayleigh number x cos ϕ).

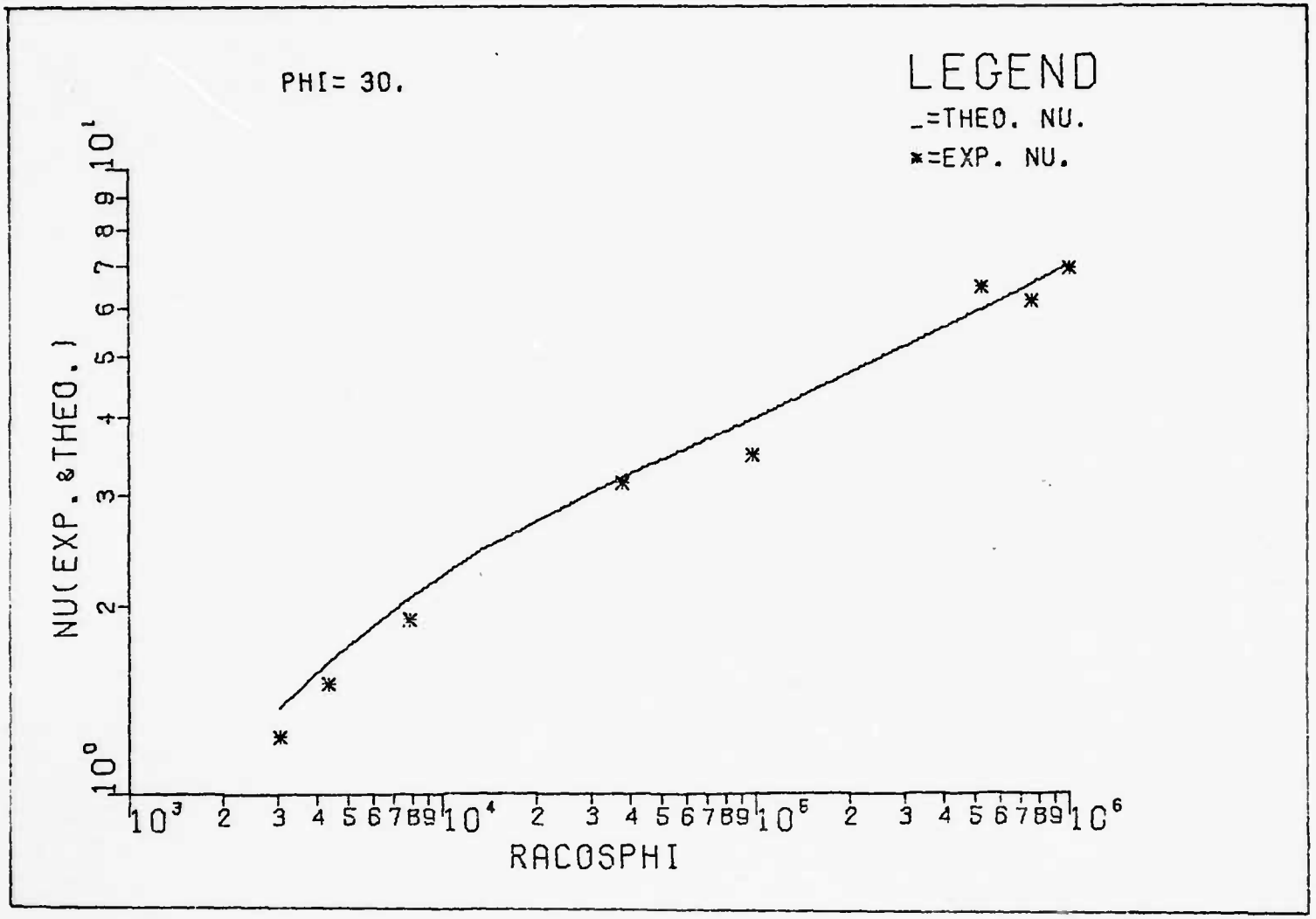

Figure 25 . A plot of theoretical and experimental Nusselt numbers vs (Rayleigh number x cos ϕ).

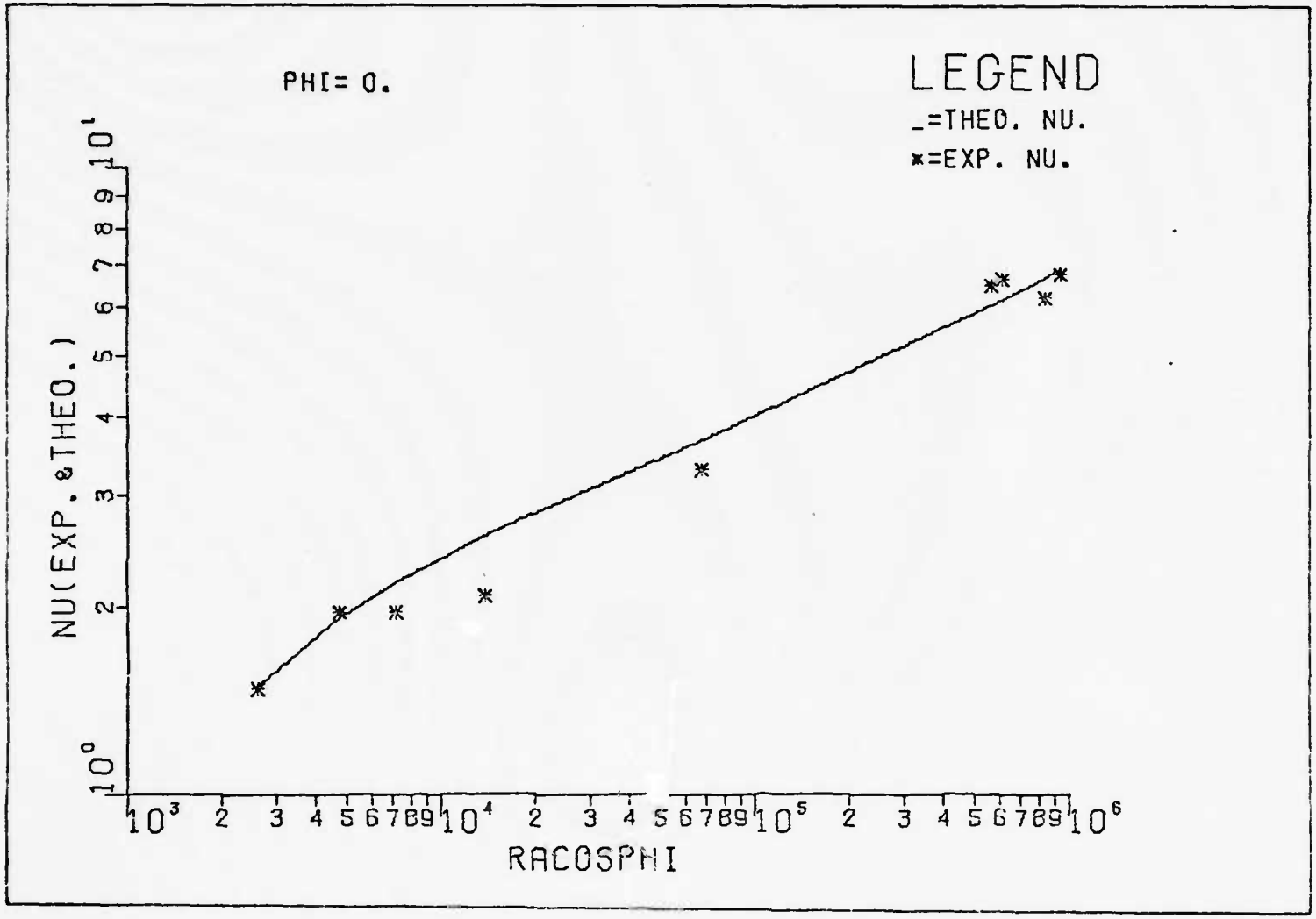

Figure 26 . A plot of theoretical and experimental Nusselt numbers vs (Rayleigh number x cos ϕ).

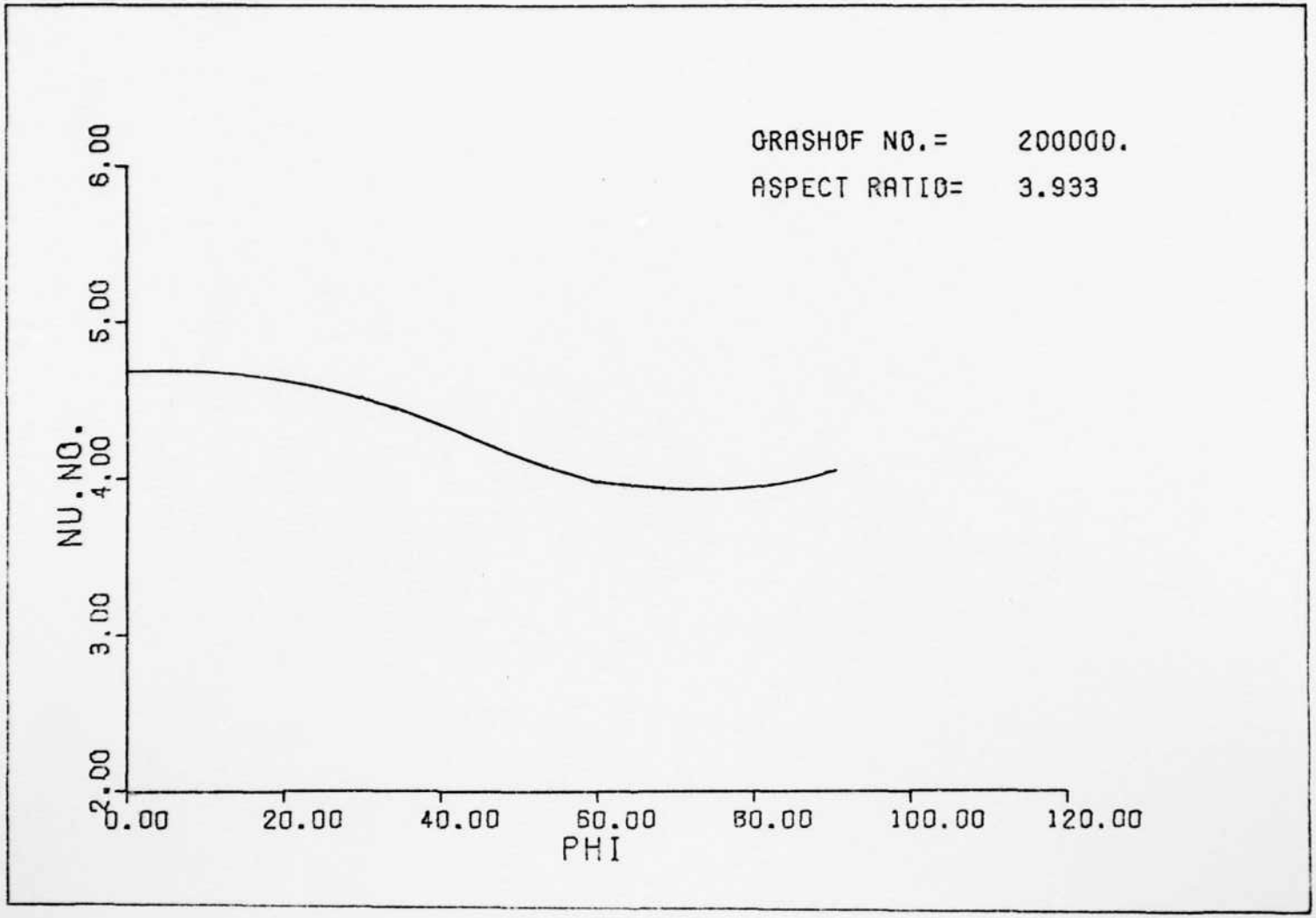

Figure 27. A Plot of Experimental Nusselt Number vs ϕ.

Partitioned Geometry

Figure 12(a) shows the interferogram of a 2.785" x 3.00" geometry with a diagonal partition.

For the partitioned case

Grashof number = 1267224.8

Average Nusselt number = 3.65

while for the case without the partition (same geometry and ϕ)

Grashof number = 1287084.4

Average Nusselt number = 8.68

It can be observed that for almost the same Grashof number the Nusselt number has been reduced by more than half.

V. Conclusions

Based on the results of this study, the following conclusions are drawn:

1. The average heat flux across a rectangular cavity, whether vertical or inclined, is primarily a function of the Grashof number or Rayleigh number.

2. For a constant Grashof number, the average heat flux across a rectangular cavity does not change appreciably by either changing the aspect ratio or the angle of inclination.

3. The correlation equations developed by Eckert for the evaluation of average heat flux across a vertical, rectangular cavity and the correlation equation developed by Hollands to determine the average heat flux across an inclined, rectangular cavity, approximate the experimental data within $\pm$ 11%, up to a Grashof number of 1.2 million.

4. The introduction of a diagonal partition into a rectangular cavity decreases the heat flux more than half.

VI. Recommendations

It is recommended that:

1. Further experimental study should be carried out on a partitioned cavity, because the introduction of a partition decreases the heat flux significantly.

2. A future study of heat flux should be carried out with the help of a Moire schlieren apparatus, which might provide a clearer fringe pattern.

References

1. Nusselt, W., Ver. deut. Ingr., Forschg. Arb., Nos. 63 and 64, 78 (1909).

2. Mull, W. and H. Reiher, Beih. Gesundh-Ing. Reihe 1, Heft 28 (1930).

3. DeGraaf, J.G.A. and E.F.M. Van der Held, Appl. Sci. Res. 3, 393 (1953).

4. Hollands, K.G.T., G. D. Raithby and L. Konicek, "Correlation Equations for Free Convection Heat Transfer in Horizontal Layers of Air and Water," International Journal of Heat and Mass Transfer, Vol. 18, 1975, pp. 879-884.

5. DeGraaf, J.G.A. and E.F.M. Van der Held, "The Relation Between the Heat Transfer and Convection Phenomena in Enclosed Plane Air Layers," Appl. Sci. Res., Vol. 3, 1953, pp. 393-409.

6. Hollands, K.G.T., T. E. Unny, G. D. Raithby and L. Konicek, "Free Convective Heat Transfer Across Inclined Air Layers," Journal of Heat Transfer, May 1976, pp. 189-193.

7. Hollands, K.G.T. and L. Konicek, "Experimental Study of the Stability of Differentially Heated Inclined Air Layers," International Journal of Heat Transfer, Vol. 16, 1973, pp. 1467-1476.

8. Eckert, E.R.G. and W. O. Carlson, "Natural Convection in Vertical Air Layer," Journal of Heat Transfer.

9. Instruction Manual of 'Precision Constant Temperature Circulating System'.

10. Aerodynamic Measurements, MIT, 1952, Chapter XII, Part I.

11. Optical Methods for Examining the Flow in High-Speed Wind Tunnels (Part II), November 1956, NATO (AGARD).

12. User's Manual of Rubicon Potentiometer.

APPENDIX A

Finite Fringe Method

Two beams of light, having sinusoidal wave patterns with the same wavelength, when combined, cancel each other if the two are out of phase by 180° and complement each other if in phase. Therefore, a series of coherent beams parallel to and in phase with each other, joining with another coherent series of beams, will produce either an area of light, or an area of dark, on a surface in their path, depending on whether the wave patterns of the two beams are in phase or out of phase by 180° when they join.

In the finite fringe mode of operation, mirrors, M_1 and M_2, and splitter plates, S_1 and S_2, (refer to Figure 7) are set at approximately 45° angles. Then, minor adjustments are made to first produce an infinite fringe pattern having equal path lengths for the test section and reference beam. The splitter plate, S_2, is then rotated through a small angle, θ, as shown in Figure 28.

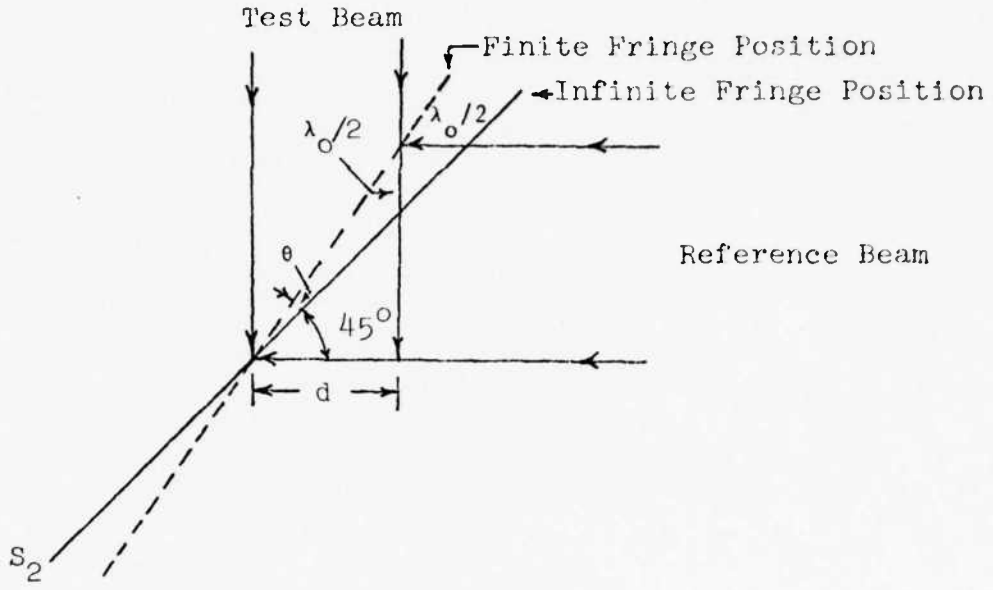

Figure 28. Test and Reference Beams in Finite Fringe Mode.

The first interference fringe, from the axis of rotation, forms where the test section beam path length has been shortened by $\lambda_o/2$, and the reference beam path length has been lengthened by $\lambda_o/2$, where λ_o is the wavelength of the reference beam of light. From the geometry in Figure 28

$$\theta = \frac{\frac{\lambda_o}{2} \cos 45^\circ}{\frac{d}{\cos 45^\circ} + \frac{\lambda_o}{2} \cos 45^\circ}$$

Now $d >> \lambda_o$, therefore the second term in the denominator can be neglected.

$$\theta = \frac{\frac{\lambda_o}{2} \cos 45^o}{\frac{d}{\cos 45^o}} = \frac{\lambda_o}{4d} \qquad \text{(A-1)}$$

An optical amplification factor, F, is defined as the ratio of the distance between fringes, d, in a finite fringe pattern, and the difference in beam path lengths between fringes, λ_o.

$$F = \frac{d}{\lambda_o} = \frac{1}{4\theta} \qquad \text{(A-2)}$$

Since $\lambda_o = C_o\tau$, the distance between finite fringes, d, can be expressed in terms of the time difference between the two beams, which is the period of the light beam, τ.

$$d = FC_o\tau \qquad \text{(A-3)}$$

Under test conditions, the difference in time for the test beam and the reference beam is changed by the change in the velocity of light in the test section.

$$\Delta\tau = \frac{L}{C_o} - \frac{L}{C} \qquad \text{(A-4)}$$

where L is the length of the test section. From equation (A-3), this time difference produces a change in fringe position, Δd

$$\Delta d = FC_o\Delta\tau \qquad \text{(A-5)}$$

Dividing Δd, equation (A-5), by d, equation (A-3); and expressing the time change as a multiple, ϵ, of the period of radiation

$$\epsilon = \frac{\Delta\tau}{\tau} = \frac{\Delta d}{d} \qquad \text{(A-6)}$$

From equation (A-4) and equation (A-6)

$$\frac{L}{C_o} - \frac{L}{C} = \varepsilon\tau = \varepsilon \frac{\lambda_{vac}}{C_{vac}} \tag{A-7}$$

Rearranging and introducing the definition of index of refraction, $n = \frac{C_{vac}}{C}$

$$(n_o - n)L = \varepsilon\lambda_{vac} \tag{A-8}$$

The index of refraction is related to gas density by the empirical Dale-Gladstone constant, K_{DG}.

$$(n_o - n) = -\rho K_{DG} \tag{A-9}$$

Combining equation (A-8) and equation (A-9)

$$\rho = -\frac{\varepsilon\lambda_{vac}}{K_{DG}L} \tag{A-10}$$

The difference in gas density between two positions in the test section, corresponding to two points on an interference fringe, depends on $\Delta\varepsilon$ between them. Let

$$\rho_1 = -\varepsilon_1 \frac{\lambda_{vac}}{K_{DG}L} \quad \text{and} \quad \rho_2 = -(\varepsilon_1 + \Delta\varepsilon) \frac{\lambda_{vac}}{K_{DG}L} \tag{A-11}$$

Then

$$\rho_2 - \rho_1 = -\Delta\varepsilon \frac{\lambda_{vac}}{K_{DG}L} \tag{A-12}$$

For an ideal gas and constant pressure

$$\frac{P}{RT_2} - \frac{P}{RT_1} = -\Delta\varepsilon \frac{\lambda_{vac}}{K_{DG}L} \tag{A-13}$$

Rearranging equation (A-13) one gets

$$T_2 = \frac{T_1}{1 - \left(\frac{R\lambda_{vac}}{PK_{DG}L}\right) \Delta\varepsilon\, T_1} \tag{A-14}$$

where from equation (A-6)

$$\Delta\epsilon = \frac{\Delta d_2 - \Delta d_1}{d} = \frac{\ell}{d} \qquad \text{(A-15)}$$

(see Figure 29)

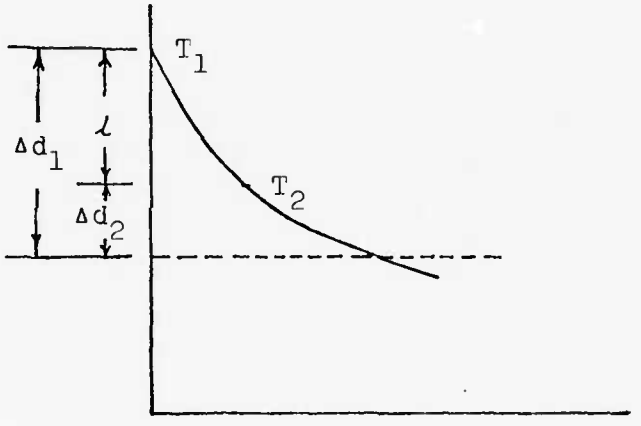

Figure 29. Deflections on an Interference Fringe.

APPENDIX B

Computer Program for Data Reduction

This program is for the calculation of the total heat transfer and local heat transfers at 20 sections of the hot plate for any of the 4 geometries having a height of 5.9" or more. For the calculation of local and total heat transfers at the cold plate, the only change required is to change the formulae for the calculation of temperatures at the first and second fringes. In that case:

$$T_2 = \frac{T_1}{1 - \epsilon_1 C_1 T_1}$$

and

$$T_3 = \frac{T_1}{1 - \epsilon_2 C_1 T_1}$$

where T_1 = temperature of the cold plate ($^{\circ}R$)

For the geometry having 2.786" height, only eight sections were used to numerically integrate the local heat transfers over the plates to calculate the total heat transfer.

Input The program requires the following parameters as input:

D = width of air layer (inches)

T_1 = temperature of the hot plate ($^{\circ}R$)

P = atmospheric pressure (pounds/ft^2)

K = thermal conductivity of air at the wall temperature (Btu/hr ft $^{\circ}F$)

CENT = width of the central section on the plate

Note: The plate has been divided into 20 sections for the purpose of numerical integration of local heat transfers on these sections to get total heat transfers. The height of these sections is as follows:

Sections 1 and 20 = 0.1 inches on picture

Sections 2-9 and 12-19 = 0.2 inches on picture

Sections 10 and 11 = "cent" inches on picture

where

$$\text{CENT} = \frac{\text{height of plate on picture} - [2(0.1)+16(0.2)]}{2} \text{ inches}$$

FF = magnification factor

$$= \frac{\text{actual height of the air layer}}{\text{height of the air layer on interferogram}}$$

L_1, L_2 = actual displacements of the first and the second fringes (inches)

= displacements on the interferogram x FF

Y_1, Y_2 = actual distances of the first and the second fringes from the wall (feet)

A listing of the program is as follows:

```
      PROGRAM TH3 (INPUT,OUTPUT)
      REAL K
      REAL L1
      REAL L2
20    READ*,D,T1,P,K,CENT,FF
      IF(D.EQ.0)GO TO 25
      N=1
5     READ*,L1,L2,Y1,Y2
      PRINT*,"L1=",L1,"L2=",L2,"Y1=",Y1,"Y2=",Y2
      EPS1=L1/D
```

```
      C1=0.026195/P
      T2=T1/(1.0+EPS1*C1*T1)
      EPS2=L2/D
      T3=T1/(1.0+EPS2*C1*T1)
      C=(Y2*(T2-T1)-Y1*(T3-T1))/((Y1-Y2)*Y1*Y2)
      B=((T2-T1)/Y1)-(C*Y1)
      QLOC=-K*B
      PRINT*,"LOCAL HEAT TRANSFER AT HOT PLATE=",QLOC
      IF(N.GT.1.AND.N.LT.10)GO TO 10
      IF(N.GE.10.AND.N.LT.12)GO TO 15
      IF(N.GE.12.AND.N.LT.20)GO TO 10
      IF(N.GE.20)GO TO 30
      QTOT=FF*0.1*QLOC/12.0
      N=N+1
      GO TO 5
   10 QTOT=QTOT+0.2*FF*QLOC/12.0
      N=N+1
      GO TO 5
   15 QTOT=QTOT+FF*CENT*QLOC/12.0
      N=N+1
      GO TO 5
   30 QTOT=QTOT+FF*0.1*QLOC/12.0
      PRINT*,"TOTAL HEAT TRANSFER AT HOT PLATE=",QTOT
      GO TO 20
   25 STOP"END OF PROGRAM"
      END
```

Appendix C

Local Heat Fluxes

1. Angle of Inclination, $\phi = 90^{o}$

Table VIII

Local Heat Fluxes for 5.93" x 0.525" Geometry
Aspect Ratio = 11.295, $\Delta T = 34.514^{o}F$, $\phi = 90^{o}$

Position Number	Distance Along the plate "x" (in)	Local Heat Fluxes at Hot Plate (Btu/hr ft²)	Local Heat Fluxes at Cold Plate (Btu/hr ft²)
1	0.0	11.8	- 6.9
2	0.324	25.6	- 4.6
3	0.648	23.8	- 6.5
4	0.972	22.0	- 7.2
5	1.296	21.2	-15.6
6	1.62	17.3	-15.3
7	1.945	10.7	-17.9
8	2.269	15.7	-12.9
9	2.593	16.1	-17.0
10	2.917	10.6	- 9.2
11	3.014	10.6	- 9.2
12	3.338	19.2	-14.2
13	3.662	14.6	-14.2
14	3.986	16.2	-32.3
15	4.310	9.8	-15.2
16	4.634	13.3	-20.7
17	4.958	7.4	-21.4
18	5.283	6.4	-23.1
19	5.607	5.1	-23.4
20	5.930	7.2	-11.3

Total Heat Transfer Rate at Hot Plate = 7.09 Btu/hr
Total Heat Transfer Rate at Cold Plate = -7.48 Btu/hr

Table IX

Local Heat Fluxes for 2.786" x 3.00" Geometry
Aspect Ratio = 0.929, $\Delta T = 38.844^{o}F$, $\phi = 90^{o}$

Position Number	Distance Along the plate "x" (in)	Local Heat Fluxes at Hot Plate (Btu/hr ft²)	Local Heat Fluxes at Cold Plate (Btu/hr ft²)
1	0.0	11.3	- 7.7
2	0.398	33.9	-14.1
3	0.796	33.4	-15.9
4	1.194	17.7	-18.2
5	1.592	20.8	-15.7
6	1.990	16.6	-28.6
7	2.388	16.2	-32.6
8	2.786	10.8	- 9.2

Total Heat Transfer Rate at Hot Plate = 4.96 Btu/hr
Total Heat Transfer Rate at Cold Plate = -4.43 Btu/hr

Table X

Local Heat Fluxes for 5.9" x 3.00" Geometry
Aspect Ratio=1.967, ΔT_1=22.51°F, ΔT_2=38.94°F, ϕ=90°

Position Number	Distance Along the plate "x" (in)	Local Heat Fluxes at Hot Plate for ΔT_1 (Btu/hr ft²)	Local Heat Fluxes at Hot Plate for ΔT_2 (Btu/hr ft²)
1	0.0	4.5	22.5
2	0.314	9.4	33.5
3	0.628	12.4	18.7
4	0.942	12.7	19.1
5	1.257	12.5	33.9
6	1.571	10.9	25.6
7	1.885	10.3	18.6
8	2.199	10.0	22.1
9	2.513	11.4	16.0
10	2.827	7.2	23.9
11	3.072	12.7	22.0
12	3.386	10.9	18.9
13	3.701	9.2	20.8
14	4.015	7.0	16.7
15	4.329	8.9	10.5
16	4.643	8.3	14.4
17	4.957	5.0	10.7
18	5.271	5.1	10.4
19	5.585	2.3	3.8
20	5.900	3.7	2.4

Total Heat Transfer Rate at Hot Plate for ΔT_1 = 4.45 Btu/hr
Total Heat Transfer Rate at Hot Plate for ΔT_2 = 9.18 Btu/hr

Table XI

Local Heat Fluxes for 5.9" x 1.5" Geometry
Aspect Ratio = 3.933, ΔT = 25.788°F, ϕ = 90°

Position Number	Distance Along the plate "x" (in)	Local Heat Fluxes at Hot Plate (Btu/hr ft²)	Local Heat Fluxes at Cold Plate (Btu/hr ft²)
1	0.0	6.2	- 2.5
2	0.318	33.9	- 1.0
3	0.635	23.9	- 1.0
4	0.952	19.8	- 3.2
5	1.270	14.5	- 3.4
6	1.587	13.6	- 4.1
7	1.905	13.3	- 4.1
8	2.222	12.2	- 6.1
9	2.540	12.0	- 8.4
10	2.857	11.9	-10.4
11	3.044	11.8	-11.2
12	3.362	8.6	-10.7
13	3.679	6.7	-12.3
14	3.997	4.3	- 6.8
15	4.314	3.5	-12.2
16	4.632	2.9	-14.0
17	4.949	2.4	-19.9
18	5.267	1.0	-22.1
19	5.584	1.2	-32.7
20	5.900	3.7	- 5.9

Total Heat Transfer Rate at Hot Plate = 5.09 Btu/hr
Total Heat Transfer Rate at Cold Plate = -4.89 Btu/hr

Table XII

Local Heat Fluxes for 5.9" x 1.50" Geometry
Aspect Ratio = 3.933, $\Delta T = 37.505^{\circ}F$, $\phi = 90^{\circ}$

Position Number	Distance Along the plate "x" (in)	Local Heat Fluxes at Hot Plate (Btu/hr ft²)	Local Heat Fluxes at Cold Plate (Btu/hr ft²)
1	0.0	3.6	- 4.2
2	0.318	42.4	- 2.9
3	0.635	31.9	- 3.5
4	0.952	35.4	- 6.7
5	1.270	30.4	- 8.2
6	1.587	31.1	-10.5
7	1.905	25.6	- 9.4
8	2.222	19.1	-11.4
9	2.540	18.7	-14.1
10	2.857	17.5	-14.7
11	3.044	15.2	-16.2
12	3.362	15.1	-20.0
13	3.680	11.9	-19.0
14	3.997	8.9	-24.1
15	4.314	8.8	-33.1
16	4.632	8.1	-26.9
17	4.949	8.1	-32.7
18	5.267	3.7	-30.0
19	5.584	3.4	-39.4
20	5.900	5.2	- 3.2

Total Heat Transfer Rate at Hot Plate = 8.87 Btu/hr
Total Heat Transfer Rate at Cold Plate = -8.52 Btu/hr

Table XIII

Local Heat Fluxes for 5.9" x 0.75" Geometry
Aspect Ratio = 7.867, ΔT = 33.818°F, ϕ = 90°

Position Number	Distance Along the plate "x" (in)	Local Heat Fluxes at Hot Plate (Btu/hr ft²)	Local Heat Fluxes at Cold Plate (Btu/hr ft²)
1	0.0	21.3	- 3.4
2	0.315	45.1	- 2.4
3	0.630	41.9	- 2.6
4	0.944	42.2	- 3.4
5	1.259	40.3	- 5.1
6	1.574	26.2	- 5.3
7	1.889	25.7	- 5.9
8	2.204	19.8	- 7.8
9	2.518	15.2	- 9.8
10	2.833	16.2	-12.2
11	3.066	12.8	-14.4
12	3.381	10.1	-15.9
13	3.696	8.0	-20.0
14	4.011	6.1	-20.5
15	4.325	5.6	-26.7
16	4.640	5.7	-43.4
17	4.955	2.3	-47.8
18	5.270	2.7	-40.3
19	5.585	3.1	-52.1
20	5.900	3.7	-20.8

Total Heat Transfer Rate at Hot Plate = 8.86 Btu/hr
Total Heat Transfer Rate at Cold Plate = -9.04 Btu/hr

2. Angle of Inclination, $\phi = 60^{o}$

Table XIV

Local Heat Fluxes for 5.93" x 0.525" Geometry
Aspect Ratio=11.295, ΔT_1=22.213°F, ΔT_2=33.873°F, ϕ=60°

Position Number	Distance Along the plate "x" (in)	Local Heat Fluxes at Hot Plate for ΔT_1 (Btu/hr ft²)	Local Heat Fluxes at Hot Plate for ΔT_2 (Btu/hr ft²)
1	0.0	7.6	7.1
2	0.324	11.5	23.3
3	0.648	12.4	44.5
4	0.972	10.1	16.1
5	1.296	10.0	12.9
6	1.620	8.9	13.9
7	1.945	6.9	12.7
8	2.269	5.4	10.9
9	2.593	5.9	10.5
10	2.917	4.5	10.9
11	3.014	5.7	10.2
12	3.338	6.5	12.4
13	3.662	7.4	11.5
14	3.986	7.0	13.0
15	4.310	7.6	10.2
16	4.634	8.1	11.0
17	4.958	7.0	8.6
18	5.283	6.8	6.6
19	5.607	3.4	5.8
20	5.930	3.7	34.2

Total Heat Transfer Rate at Hot Plate for ΔT_1 = 3.64 Btu/hr
Total Heat Transfer Rate at Hot Plate for ΔT_2 = 6.84 Btu/hr

Table XV

Local Heat Fluxes for 2.786" x 3.00" Geometry
Aspect Ratio = 0.929, $\Delta T = 26.375^{o}F$, $\phi = 60^{o}$

Position Number	Distance Along the plate "x" (in)	Local Heat Fluxes at Hot Plate (Btu/hr ft²)	Local Heat Fluxes at Cold Plate (Btu/hr ft²)
1	0.0	1.8	- 0.7
2	0.398	13.5	- 3.4
3	0.796	14.0	- 8.1
4	1.194	13.7	-10.3
5	1.592	9.3	-14.0
6	1.990	5.8	-13.7
7	2.388	4.3	-13.7
8	2.786	1.1	- 1.7

Total Heat Transfer Rate at Hot Plate = 2.06 Btu/hr
Total Heat Transfer Rate at Cold Plate = -2.14 Btu/hr

Table XVI

Local Heat Fluxes for 2.786" x 3.00" Geometry
Aspect Ratio = 0.929, $\Delta T = 49.859^{\circ}F$, $\phi = 60^{\circ}$

Position Number	Distance Along the plate "x" (in)	Local Heat Fluxes at Hot Plate (Btu/hr ft²)	Local Heat Fluxes at Cold Plate (Btu/hr ft²)
1	0.0	0.9	- 6.5
2	0.398	23.9	-12.0
3	0.796	27.0	-14.8
4	1.194	20.8	-18.5
5	1.592	20.5	-21.3
6	1.990	13.8	-25.6
7	2.388	12.4	-24.9
8	2.786	7.0	- 1.4

Total Heat Transfer Rate at Hot Plate = 4.06 Btu/hr
Total Heat Transfer Rate at Cold Plate = -4.02 Btu/hr

Table XVII

Local Heat Fluxes for 5.9" x 3.00 Geometry
Aspect Ratio = 1.967, ΔT = 18.849°F, ϕ = 60°

Position Number	Distance Along the plate "x" (in)	Local Heat Fluxes at Hot Plate (Btu/hr ft²)
1	0.0	3.6
2	0.314	3.7
3	0.628	8.7
4	0.942	9.3
5	1.257	8.8
6	1.571	7.3
7	1.885	7.4
8	2.199	6.4
9	2.513	2.3
10	2.827	4.4
11	3.072	5.0
12	3.386	7.3
13	3.701	7.1
14	4.015	7.9
15	4.329	6.2
16	4.643	7.3
17	4.957	4.8
18	5.271	3.8
19	5.585	2.7
20	5.900	1.6

Total Heat Transfer Rate at Hot Plate = 2.96 Btu/hr

Table XVIII

Local Heat Fluxes for 5.9" x 1.5" Geometry
Aspect Ratio=3.933, ΔT_1=20.522°F, ΔT_2=38.566°F, ϕ=60°

Position Number	Distance Along the plate "x" (in)	Local Heat Fluxes at Hot Plate for ΔT_1 (Btu/hr ft²)	Local Heat Fluxes at Hot Plate for ΔT_2 (Btu/hr ft²)
1	0.0	2.0	5.7
2	0.318	15.2	58.7
3	0.635	13.8	58.6
4	0.952	13.8	36.9
5	1.270	6.8	24.1
6	1.587	7.5	10.3
7	1.905	5.3	11.5
8	2.222	8.3	5.2
9	2.540	8.4	8.4
10	2.857	6.8	14.5
11	3.044	5.2	14.5
12	3.362	5.5	10.0
13	3.679	5.5	8.7
14	3.997	6.1	14.5
15	4.314	3.6	9.7
16	4.632	2.6	5.7
17	4.949	3.4	5.8
18	5.267	2.0	5.9
19	5.584	1.9	1.9
20	5.900	8.2	8.1

Total Heat Transfer Rate at Hot Plate for ΔT_1 = 3.31 Btu/hr
Total Heat Transfer Rate at Hot Plate for ΔT_2 = 8.15 Btu/hr

Table XIX

Local Heat Fluxes for 5.9" x 0.75" Geometry
Aspect Ratio=7.867, ΔT_1=21.962°F, ΔT_2=37.435°F, ϕ=60°

Position Number	Distance Along the plate "x" (in)	Local Heat Fluxes at Hot Plate for ΔT_1 (Btu/hr ft²)	Local Heat Fluxes at Hot Plate for ΔT_2 (Btu/hr ft²)
1	0.0	3.4	0.0
2	0.315	22.9	71.3
3	0.630	18.0	35.8
4	0.944	17.3	27.9
5	1.259	12.4	21.2
6	1.574	12.2	15.5
7	1.889	8.1	15.2
8	2.204	6.8	14.0
9	2.518	5.4	15.1
10	2.833	6.7	14.4
11	3.066	6.4	11.7
12	3.381	6.5	11.5
13	3.696	5.6	8.2
14	4.011	5.0	8.4
15	4.325	5.2	8.2
16	4.640	3.1	3.2
17	4.955	2.3	3.0
18	5.270	1.6	3.4
19	5.585	1.0	1.2
20	5.900	5.9	9.0

Total Heat Transfer Rate at Hot Plate for ΔT_1 = 3.92 Btu/hr
Total Heat Transfer Rate at Hot Plate for ΔT_2 = 7.62 Btu/hr

3. Angle of Inclination, $\phi = 30^{\circ}$

Table XX

Local Heat Fluxes for 5.93" x 0.525" Geometry
Aspect Ratio=11.295, ΔT_1=26.151°F, ΔT_2=39.00°F, ϕ=30°

Position Number	Distance Along the plate "x" (in)	Local Heat Fluxes at Hot Plate for ΔT_1 (Btu/hr ft²)	Local Heat Fluxes at Hot Plate for ΔT_2 (Btu/hr ft²)
1	0.0	14.1	25.9
2	0.324	15.7	32.3
3	0.648	14.0	20.9
4	0.972	12.0	17.5
5	1.296	11.7	16.1
6	1.620	8.5	17.3
7	1.945	8.4	16.2
8	2.269	15.8	20.8
9	2.593	14.2	25.9
10	2.917	13.0	28.4
11	3.014	9.5	20.8
12	3.338	6.9	16.8
13	3.662	7.6	18.4
14	3.986	9.5	17.7
15	4.310	14.1	18.3
16	4.634	11.3	30.3
17	4.958	9.2	22.3
18	5.283	9.5	15.0
19	5.607	5.0	5.8
20	5.930	9.4	20.6

Total Heat Transfer Rate at Hot Plate for ΔT_1 = 5.29 Btu/hr
Total Heat Transfer Rate at Hot Plate for ΔT_2 = 9.73 Btu/hr

Table XXI

Local Heat Fluxes for 2.786" x 3.00" Geometry
Aspect Ratio = 0.929, $\Delta T = 39.753^{\circ}F$, $\phi = 30^{\circ}$

Position Number	Distance Along the plate "x" (in)	Local Heat Fluxes at Hot Plate (Btu/hr ft²)	Local Heat Fluxes at Cold Plate (Btu/hr ft²)
1	0.0	2.3	- 2.7
2	0.398	13.5	-11.8
3	0.796	17.3	-17.1
4	1.194	22.2	-19.5
5	1.592	20.8	-18.1
6	1.990	15.4	-19.0
7	2.388	12.4	-12.8
8	2.786	4.0	- 2.0

Total Heat Transfer Rate at Hot Plate = 3.47 Btu/hr
Total Heat Transfer Rate at Cold Plate = -3.33 Btu/hr

Table XXII

Local Heat Fluxes for 2.786" x 3.00" Geometry
Aspect Ratio = 0.929, ΔT = 53.569°F, ϕ = 30°

Position Number	Distance Along the plate "x" (in)	Local Heat Fluxes at Hot Plate (Btu/hr ft²)	Local Heat Fluxes at Cold Plate (Btu/hr ft²)
1	0.0	2.9	- 2.4
2	0.398	41.7	- 9.1
3	0.796	36.0	-17.3
4	1.194	25.6	-21.0
5	1.592	18.4	-26.2
6	1.990	18.6	-34.0
7	2.388	11.4	-43.6
8	2.786	3.8	- 2.0

Total Heat Transfer Rate at Hot Plate = 5.41 Btu/hr
Total Heat Transfer Rate at Cold Plate = -5.09 Btu/hr

Table XXIII

Local Heat Fluxes for 5.9" x 3.00" Geometry
Aspect Ratio = 1.967, ΔT = 25.035°F, ϕ = 30°

Position Number	Distance Along the plate "x" (in)	Local Heat Fluxes at Hot Plate (Btu/hr ft²)
1	0.0	4.5
2	0.314	11.5
3	0.628	16.8
4	0.942	13.1
5	1.257	14.4
6	1.571	13.2
7	1.885	11.4
8	2.199	7.6
9	2.513	8.4
10	2.827	6.6
11	3.072	9.7
12	3.386	10.8
13	3.701	10.8
14	4.015	9.3
15	4.329	7.3
16	4.643	8.6
17	4.957	8.8
18	5.271	5.9
19	5.585	4.7
20	5.900	4.4

Total Heat Transfer Rate at Hot Plate = 4.80 Btu/hr

AD-A094 759 AIR FORCE INST OF TECH WRIGHT-PATTERSON AFB OH SCHOO--ETC F/G 20/13
A STUDY OF FREE CONVECTION IN AN INCLINED, RECTANGULAR CAVITY.(U)
DEC 80 M K KHAN
UNCLASSIFIED AFIT/GAE/AA/80D-13 NL

2 OF 2
AD
A094759

END
DATE FILMED
3-81
DTIC

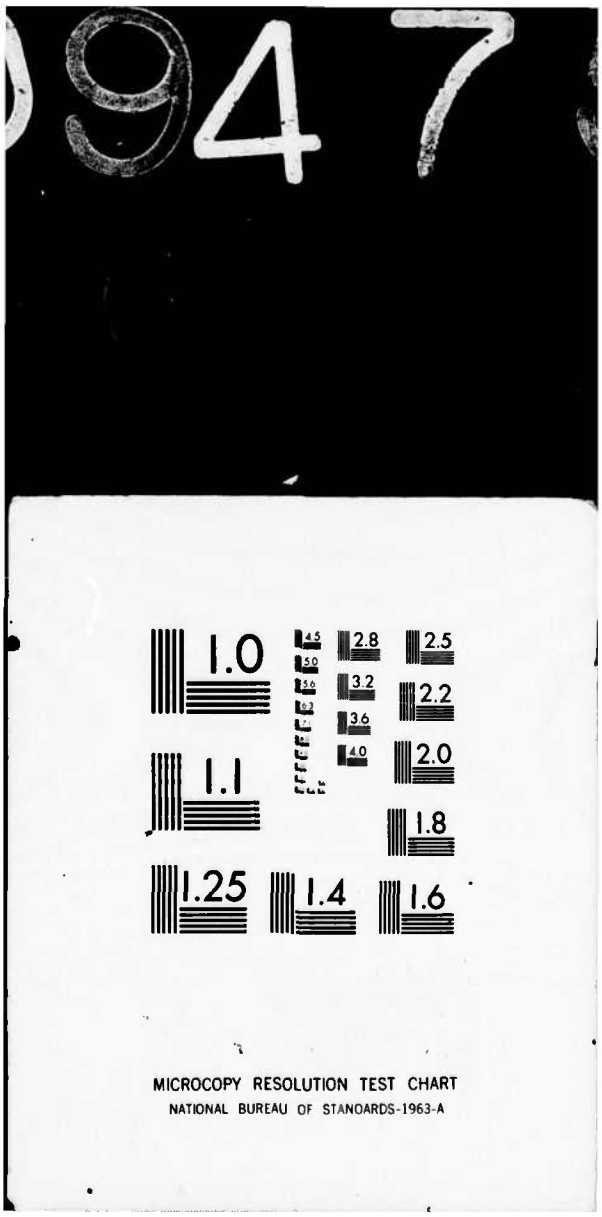
947
1.0
1.1
1.25
1.4
1.6
1.8
2.0
2.2
2.5
2.8
3.2
3.6
4.0
MICROCOPY RESOLUTION TEST CHART
NATIONAL BUREAU OF STANOARDS-1963-A

Table XXIV

Local Heat Fluxes for 5.9" x 1.5" Geometry
Aspect Ratio=3.933, ΔT_1=13.435°F, ΔT_2=39.64°F, ϕ=30°

Position Number	Distance Along the plate "x" (in)	Local Heat Fluxes at Hot Plate for ΔT_1 (Btu/hr ft²)	Local Heat Fluxes at Hot Plate for ΔT_2 (Btu/hr ft²)
1	0.0	2.8	7.9
2	0.318	12.2	42.0
3	0.635	13.0	34.1
4	0.952	8.4	28.5
5	1.270	7.8	29.0
6	1.587	9.3	20.9
7	1.905	7.1	20.5
8	2.222	5.1	15.8
9	2.540	3.5	16.2
10	2.857	3.5	11.5
11	3.044	3.1	13.0
12	3.362	3.0	12.0
13	3.679	3.1	13.5
14	3.997	2.8	13.9
15	4.314	2.9	10.5
16	4.632	2.5	8.5
17	4.949	2.2	7.7
18	5.267	2.1	7.0
19	5.584	0.5	3.3
20	5.900	0.7	0.6

Total Heat Transfer Rate at Hot Plate for ΔT_1 = 2.46 Btu/hr
Total Heat Transfer Rate at Hot Plate for ΔT_2 = 8.17 Btu/hr

Table XXV

Local Heat Fluxes for 5.9" x 0.75" Geometry
Aspect Ratio = 7.867, ΔT = 23.803°F, ϕ = 30°

Position Number	Distance Along the plate "x" (in)	Local Heat Fluxes at Hot Plate (Btu/hr ft²)
1	0.0	5.0
2	0.315	29.8
3	0.630	16.6
4	0.944	14.4
5	1.259	12.3
6	1.574	10.3
7	1.889	10.4
8	2.204	9.4
9	2.518	10.4
10	2.833	10.3
11	3.066	9.7
12	3.381	11.2
13	3.696	12.7
14	4.011	13.1
15	4.325	9.9
16	4.640	10.1
17	4.955	5.5
18	5.270	2.8
19	5.585	2.2
20	5.900	7.5

Total Heat Transfer Rate at Hot Plate = 5.36 Btu/hr

4. Angle of Inclination, $\phi = 0^{o}$

Table XXVI

Local Heat Fluxes for 5.93" x 0.525" Geometry
Aspect Ratio=11.295, ΔT_1=19.347°F, ΔT_2=37.869°F, ϕ=0°

Position Number	Distance Along the plate "x" (in)	Local Heat Fluxes at Hot Plate for ΔT_1 (Btu/hr ft²)	Local Heat Fluxes at Hot Plate for ΔT_2 (Btu/hr ft²)
1	0.0	10.3	22.6
2	0.324	8.8	29.6
3	0.648	8.1	34.3
4	0.972	7.0	32.6
5	1.296	10.4	24.5
6	1.620	12.2	29.7
7	1.945	10.1	27.2
8	2.269	10.7	36.8
9	2.593	10.7	34.8
10	2.917	10.3	25.1
11	3.014	10.7	24.8
12	3.338	10.7	24.9
13	3.662	12.1	28.6
14	3.986	12.1	25.3
15	4.310	5.7	23.7
16	4.634	8.5	23.1
17	4.958	9.0	23.1
18	5.283	10.2	12.4
19	5.607	7.2	5.7
20	5.930	10.0	10.6

Total Heat Transfer Rate at Hot Plate for ΔT_1 = 4.7 Btu/hr
Total Heat Transfer Rate at Hot Plate for ΔT_2 = 12.33 Btu/hr

Table XVII

Local Heat Fluxes for 2.786" x 3.00" Geometry
Aspect Ratio = 0.929, $\Delta T = 25.00^{\circ}F$, $\phi = 0^{\circ}$

Position Number	Distance Along the plate "x" (in)	Local Heat Fluxes at Hot Plate (Btu/hr ft²)	Local Heat Fluxes at Cold Plate (Btu/hr ft²)
1	0.0	7.2	- 2.7
2	0.398	14.1	-10.5
3	0.796	10.6	-11.9
4	1.194	6.9	-10.2
5	1.592	8.7	- 7.3
6	1.990	11.2	-11.5
7	2.388	10.4	-14.7
8	2.786	3.0	- 6.5

Total Heat Transfer Rate at Hot Plate = 2.22 Btu/hr
Total Heat Transfer Rate at Cold Plate = -2.35 Btu/hr

Table XVIII

Local Heat Fluxes for 2.786" x 3.00" Geometry
Aspect Ratio = 0.929, $\Delta T = 40.073^{o}F$, $\phi = 0^{o}$

Position Number	Distance Along the plate "x" (in)	Local Heat Fluxes at Hot Plate (Btu/hr ft²)	Local Heat Fluxes at Cold Plate (Btu/hr ft²)
1	0.0	0.8	- 3.8
2	0.398	24.3	-18.0
3	0.796	18.3	- 9.0
4	1.194	19.8	-18.3
5	1.592	17.0	-20.5
6	1.990	18.9	-20.5
7	2.388	16.3	-24.5
8	2.786	5.7	- 0.3

Total Heat Transfer Rate at Hot Plate = 3.90 Btu/hr
Total Heat Transfer Rate at Cold Plate = -3.68 Btu/hr

Table XXIX

Local Heat Fluxes for 5.9" x 3.00" Geometry
Aspect Ratio=1.967, ΔT_1=22.455°F, ΔT_2=35.478°F, ϕ=0°

Position Number	Distance Along the plate "x" (in)	Local Heat Fluxes at Hot Plate for ΔT_1 (Btu/hr ft²)	Local Heat Fluxes at Hot Plate for ΔT_2 (Btu/hr ft²)
1	0.0	3.4	2.4
2	0.314	10.3	15.1
3	0.628	10.6	11.5
4	0.942	6.0	13.2
5	1.257	9.1	8.0
6	1.571	9.1	4.0
7	1.885	10.1	4.0
8	2.199	9.2	4.0
9	2.513	9.2	8.0
10	2.827	6.0	13.2
11	3.072	7.5	19.0
12	3.386	8.3	20.6
13	3.701	9.4	20.4
14	4.015	11.7	22.5
15	4.329	11.8	22.0
16	4.643	9.4	20.7
17	4.957	4.6	19.2
18	5.271	8.8	10.5
19	5.585	8.2	8.2
20	5.900	4.4	11.3

Total Heat Transfer Rate at Hot Plate for ΔT_1 = 4.28 Btu/hr
Total Heat Transfer Rate at Hot Plate for ΔT_2 = 6.55 Btu/hr

Table XXX

Local Heat Fluxes for 5.9" x 1.5" Geometry
Aspect Ratio = 3.933, ΔT = 21.818°F, ϕ = 0°

Position Number	Distance Along the plate "x" (in)	Local Heat Fluxes at Hot Plate (Btu/hr ft²)
1	0.0	4.9
2	0.318	16.3
3	0.635	13.9
4	0.952	8.1
5	1.270	9.0
6	1.587	8.2
7	1.905	6.2
8	2.222	6.0
9	2.540	6.0
10	2.857	6.1
11	3.044	7.4
12	3.362	7.4
13	3.679	7.7
14	3.997	9.1
15	4.314	10.3
16	4.632	11.1
17	4.949	10.0
18	5.267	7.4
19	5.584	6.3
20	5.900	4.2

Total Heat Transfer Rate at Hot Plate = 4.21 Btu/hr

Table XXXI

Local Heat Fluxes for 5.9" x 0.75" Geometry
Aspect Ratio=7.867, ΔT_1=18.803°F, ΔT_2=38.304°F, ϕ=0°

Position Number	Distance Along the plate "x" (in)	Local Heat Fluxes at Hot Plate for ΔT_1 (Btu/hr ft²)	Local Heat Fluxes at Hot Plate for ΔT_2 (Btu/hr ft²)
1	0.0	1.9	2.4
2	0.315	12.7	22.0
3	0.630	9.6	26.7
4	0.944	10.1	24.2
5	1.259	11.7	27.0
6	1.574	9.3	19.1
7	1.889	9.0	18.4
8	2.204	9.9	18.9
9	2.518	9.3	24.9
10	2.833	9.1	19.6
11	3.066	9.5	20.0
12	3.381	10.2	12.8
13	3.696	9.8	18.5
14	4.011	6.6	18.9
15	4.325	7.9	18.1
16	4.640	8.7	19.5
17	4.955	9.1	20.7
18	5.270	8.3	22.2
19	5.585	5.2	13.5
20	5.900	4.0	5.4

Total Heat Transfer Rate at Hot Plate for ΔT_1 = 4.36 Btu/hr
Total Heat Transfer Rate at Hot Plate for ΔT_2 = 9.52 Btu/hr

Table XXXII

Local Heat Fluxes for 2.825" x 3.05" Geometry
With Diagonal Partition
Aspect Ratio = 0.926, ΔT = 39.355°F, ϕ = 90°

Position Number	Distance Along the plate "x" (in)	Local Heat Fluxes at Hot Plate (Btu/hr ft²)	Local Heat Fluxes at Cold Plate (Btu/hr ft²)
1	0.0	0.9	0.0
2	0.327	18.8	- 4.0
3	0.653	15.8	- 2.4
4	0.980	10.6	- 5.6
5	1.306	9.6	- 9.2
6	1.519	8.6	-10.5
7	1.845	7.1	-12.1
8	2.172	1.8	-13.9
9	2.498	6.1	-18.0
10	2.825	0.0	- 0.9

Total Heat Transfer Rate at Hot Plate = 2.06 Btu/hr
Total Heat Transfer Rate at Cold Plate = -1.98 Btu/hr

Vita

Flight Lieutenant Mohammad Khalid Khan was born on November 22, 1951, in Mardan, Pakistan, the son of Mohammad Akbar Khan. After completing the F. Sc. (pre-engineering) certificate from Cadet College, Hasan Abdal, in July 1969, he joined the Pakistan Air Force as a cadet at the College of Aeronautical Engineering, Korangi Creek, Karachi. He graduated from the same college in January 1975 with a degree of Bachelor of Engineering (with distinction) in in Aerospace Engineering and commissioned in the Air Force as a Flying Officer. He was assigned various engineering and maintenance jobs in the operational units of the Pakistan Air Force. In May 1979, he was selected for the Master's program in aeronautical engineering at the United States Air Force Institute of Technology, Wright-Patterson Air Force Base, Ohio.

Permanent Address: c/o Mr. Ozair Siddiqui
A-282; Block 5
Gulshen-i-Iqbal
Karachi
Pakistan

(This thesis was typed by Mrs. Clarinda Collins)

UNCLASSIFIED

SECURITY CLASSIFICATION OF THIS PAGE (When Data Entered)

REPORT DOCUMENTATION PAGE	READ INSTRUCTIONS BEFORE COMPLETING FORM
1. REPORT NUMBER: AFIT/GAE/AA/80D-13	2. GOVT ACCESSION NO.: AD-A094 759
	3. RECIPIENT'S CATALOG NUMBER
4. TITLE (and Subtitle): A STUDY OF FREE CONVECTION IN AN INCLINED, RECTANGULAR CAVITY	5. TYPE OF REPORT & PERIOD COVERED: MS Thesis
	6. PERFORMING ORG. REPORT NUMBER
7. AUTHOR(s): Mohammad Khalid Khan, Flt Lt PAF	8. CONTRACT OR GRANT NUMBER(s)
9. PERFORMING ORGANIZATION NAME AND ADDRESS: Air Force Institute of Technology (AFIT/EN) Wright-Patterson AFB OH 45433	10. PROGRAM ELEMENT, PROJECT, TASK AREA & WORK UNIT NUMBERS
11. CONTROLLING OFFICE NAME AND ADDRESS: Department of Aeronautics and Astronautics Air Force Institute of Technology Wright-Patterson AFB OH 45433	12. REPORT DATE: December 1980
	13. NUMBER OF PAGES: 104
14. MONITORING AGENCY NAME & ADDRESS(if different from Controlling Office)	15. SECURITY CLASS. (of this report): Unclassified
	15a. DECLASSIFICATION/DOWNGRADING SCHEDULE

16. DISTRIBUTION STATEMENT (of this Report)

Approved for public release; distribution unlimited.

17. DISTRIBUTION STATEMENT (of the abstract entered in Block 20, if different from Report)

18. SUPPLEMENTARY NOTES: Approved for public release; IAW AFR 190-17

FREDRIC C. LYNCH, Major, USAF
Director of Public Affairs
30 DEC 1980

19. KEY WORDS (Continue on reverse side if necessary and identify by block number)

Free Convection
Inclined, Rectangular Cavity
High Grashof Numbers

20. ABSTRACT (Continue on reverse side if necessary and identify by block number)

A small experimental apparatus was designed for the measurement of heat flux across an enclosed, rectangular air cavity, which could be placed at any angle of inclination. The heat flux evaluation was done with the help of an interferometer. Heat flux was determined for five aspect ratios, each placed at four different angles and two different temperature differences for each setting. The average Nusselt number was found to be primarily a function of Grashof number or Rayleigh number. Three correlation

DD FORM 1 JAN 73 1473 EDITION OF 1 NOV 65 IS OBSOLETE

UNCLASSIFIED

SECURITY CLASSIFICATION OF THIS PAGE (When Data Entered)

Block #20 (continued)

equations developed by earlier studies are fitted to the data. The correlation equations are found to approximate the heat flux within $\pm$ 11%, up to a Grashof number of 1.2 million.

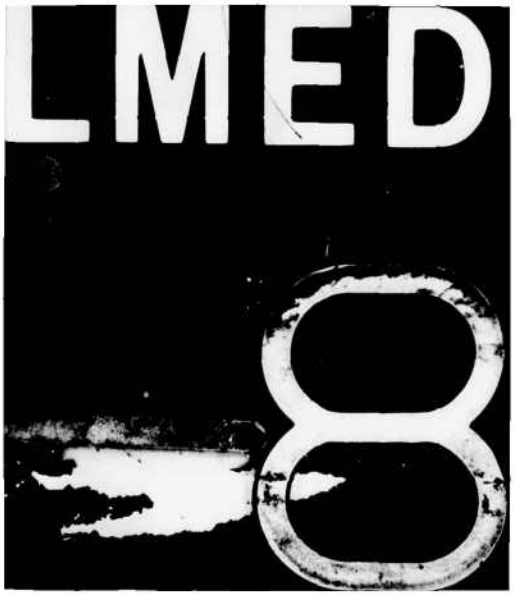
LMED
8